2004

# Design and performance of electric shock absorber

Oly D. Paz
*Louisiana State University and Agricultural and Mechanical College*

# DESIGN AND PERFORMANCE OF ELECTRIC SHOCK ABSORBER

A Thesis

Submitted to the Graduate Faculty of the
Louisiana State University and
Agricultural and Mechanical College
in partial fulfillment of the
requirements for the degree of
Master of Science in Electrical Engineering

in

The Department of Electrical and Computer Engineering

by
Oly D. Paz
B.S. Universidad del Zulia, 1990
December 2004

## ACKNOWLEGMENTS

I would like to thank Dr. Ernest Mendrela, my major professor for his valuable suggestions and support.

It is important to mention the support of my family, especially that of my husband who has encouraged me to continue with this project.

Author

## TABLE OF CONTENTS

## LIST OF TABLES

## LIST OF FIGURES

## ABSTRACT

The electric shock absorber is a device that converts the kinetic energy of an oscillating object into electric energy. This kinetic energy is normally dumped in a form of thermal energy in a conventional, mechanical shock absorber. The electric shock absorber consists of a permanent magnet linear synchronous generator (PMLSG), a spring, and an electric energy accumulator.

The major goal of the project is to design and analyze the operation of an electric shock absorber. In order to define the initial requirements that the electric shock absorber has to satisfy, the construction and performance of currently used shock absorbers were studied first. With respect to this study, five versions of PMLSG were analyzed qualitatively and the most suitable design was selected.

The next subject was the design calculations for the chosen type of PMLSG. To determine the dimensions as well as the parameters of its magnetic and electric circuits, the calculation program was written using MATLAB.

The designed PMLSG was studied under steady-state conditions to determine its electromechanical characteristics. For this purpose the mathematical model of the generator was proposed and a program was written in MATLAB that allowed calculating its output parameters under different operation conditions.

The PMLSG operates practically in dynamic conditions within the whole system: generator – spring – controlled rectified – battery. The dynamic model of the entire system of the electric shock absorber was proposed and described using the voltage equilibrium equation for the electrical port and the force equilibrium equation for the mechanical port. On the basis of these equations, a block diagram was built and simulations were carried out by using MATLAB-SIMULINK. The performance of the electric shock absorber obtained from simulations was compared with mechanical parameters of the mechanical shock absorber. The conclusion obtained indicates that the electric shock absorber is able to store part of the recovered energy in the battery. However, a great part of this energy is lost in the generator resistance and in the external resistance, which is necessary to be connected to the generator output terminal in order to obtain the desire electromechanical parameters.

# CHAPTER 1
# INTRODUCTION

Shocks absorbers are used to damp oscillations by absorbing the energy contained in the springs or torsion bars when the wheels of an automobile move up and down. Conventional shock absorbers do not support vehicle weight. They reduce the dynamic wheel-load variations and prevent the wheels from lifting off the road surface except on extremely rough surfaces and making possible much more precise steering and braking. The shock absorbers turn the kinetic energy of suspension motion into thermal energy, or heat energy, to be dissipated through the hydraulic fluid, [1] [2]. However, this kinetic energy can be converted into electric energy, which in turn can be stored in a battery. This is possible if an electric shock absorber is used. This is particularly important if an electric vehicle is considered. By converting the oscillation energy and storing it in the battery, the overall efficiency of the electric drive is increasing. The energy in turn, contributes to the extension of the driving distance under the single charge.

So far there has not been any publication on electric shock absorber, except "Electric Shock Absorber for Electric Vehicles," by Mendrela [3]. This paper was the only one that presented an idea of such an electromechanical shock absorber.

A subject of this project is one of a few design versions of the electric shock absorbers. The objectives of the project are:

1) A review of the currently used shock absorbers in terms of their performance characteristics.
2) A qualitative comparative study of different types of electric shock absorbers and a selection of the most suitable design.
3) Design calculations in order to determine the main design parameters of the selected version.
4) Simulation of dynamics of electric shock absorber in order to determine its electromechanical performance.

# CHAPTER 2
# CURRENTLY USED SHOCK ABSORBERS

The amount of resistance a shock absorber develops depends on the speed of the suspension and the number and size of the holes of the piston. All modern shock absorbers are velocity sensitive hydraulic damping devices. This means that the faster the suspension moves the more resistance the shock absorber provides. Because of this feature, shock absorbers adjust themselves to road conditions. As a result, shock absorbers reduce the rate of:

- Bounce
- Roll or sway
- Brake dive and acceleration squat

At present there are in use two kinds of shock absorber designs: twin-tube and single-tube shock absorbers.

## 2.1 Twin - Tube Design

Many types of twin-tube shock absorbers exist today. The scheme of one of them is shown in Fig. 2.1. It has an inner tube known as the working or pressure tube 5 and an outer tube 6, known as the reserve tube. The outer tube 6 is used to store the excess hydraulic fluid**.**

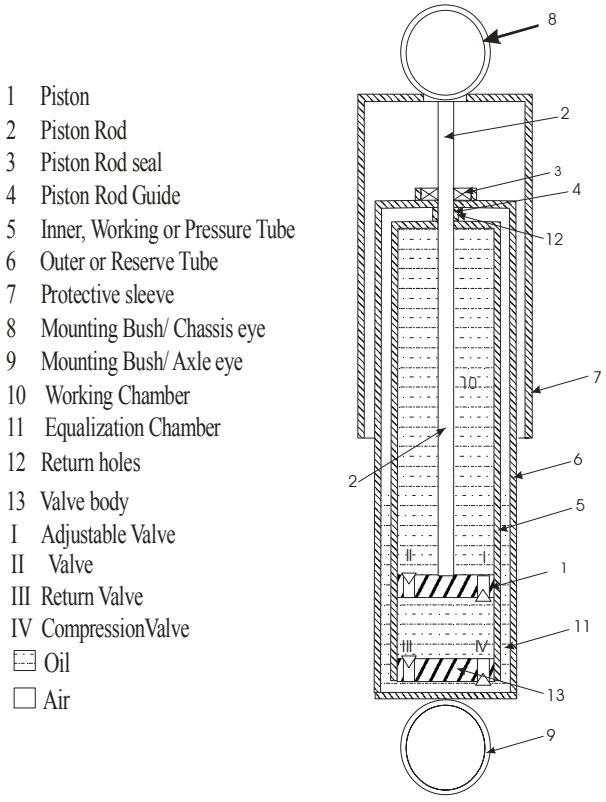


Fig. 2.1. Diagram of a twin–tube shock absorber [1].

When the wheels are subject to bump, piston 1 moves down and part of the oil flows out of the lower working chamber 10 through the valve II into the upper chamber 10. The oil goes to the equalization Chamber 11 through the base valve IV in the valve body 13. The valve VI is called a compression valve, and it is located at the bottom of the pressure tube. It controls fluid movement during the compression cycle. This produces the main forces necessary for the compression damping and only if this does not suffice can the valve II on the piston valve become effective.

When the axle rebounds, there is overpressure between the piston 1 and the piston rod guide 4. As this happens, the main oil volume is pushed to the adjustable valve I, which causes the jounce damping. The minor fluid is squeezed through the gap between the guide 4 and the piston rod 2. If the rod extends, this leads to a lack of oil in the working chamber 10. The missing liquid is sucked from the equalization chamber 11 and flows through the return valve III, which is also only a simple return valve. The oil is pulsing back and forth between the working chamber 10 and equalization chamber 11 is cooled in the outer tube 6.

Notice, that the piston rod 2 passes through a rod guide 4 and a seal 3 at the upper end of the pressure tube. The rod guide 4 keeps the rod 2 in line with the pressure tube 5 and allows the piston 1 to move freely inside. The seal 3 keeps the hydraulic oil inside and contamination out.

Bore size is the diameter of the piston 1 and the inside of the pressure tube. Generally, the larger the unit, the higher the potential control levels are because of the larger piston displacement and pressure areas. The larger the piston area, the lower the internal operating pressure and temperature. This design provides higher damping capabilities.

Ride engineers select valve values for a particular vehicle to achieve optimal ride characteristics of balance and stability under a wide variety of driving conditions. Their selection of valve springs and holes control fluid flow within the unit, which determines the feeling and handling of the vehicle.

In most of the twin–tube shock absorbers, the rubber bushings between the shock absorber and the frame of suspension are used to reduce transmitted road noise and suspension vibration. The rubber bushings are flexible in order to allow movement during travel. The upper part of the shock absorber is connected to the vehicle frame.

## 2.2 Single - Tube Design

The scheme of a single–tube shock absorber is shown in Fig. 2.2. It consists of only one high–pressure tube. Inside the pressure tube 4 there are two pistons: a dividing piston 1 and a working piston 2. Gas and oil are separated by the piston 1, which seals off the actual working chamber 8. The working piston 2 carries the valves 10 and 11. At the top is the equalization chamber 9. The piston rod 3 can extend upward and downward. The pressure tube 4 of the single–tube design is larger than a twin tube design to accommodate for dead length. The working piston 2 and the rod piston 3 are very similar to the pistons of the twin tube shock absorber.

The equalization chamber 9 must absorb the volume equalization by the oil warming, and the volume displaced by the piston rod 3. The area above the dividing piston 1 is pressurized to about 360 psi with nitrogen gas. This gas pressure helps support some of the vehicle's weight. The oil is located in the area below the piston.

During operation, the dividing piston 1 moves up and down as the piston rod 3 moves in and out of the shock absorber, keeping the pressure tube full at all times.

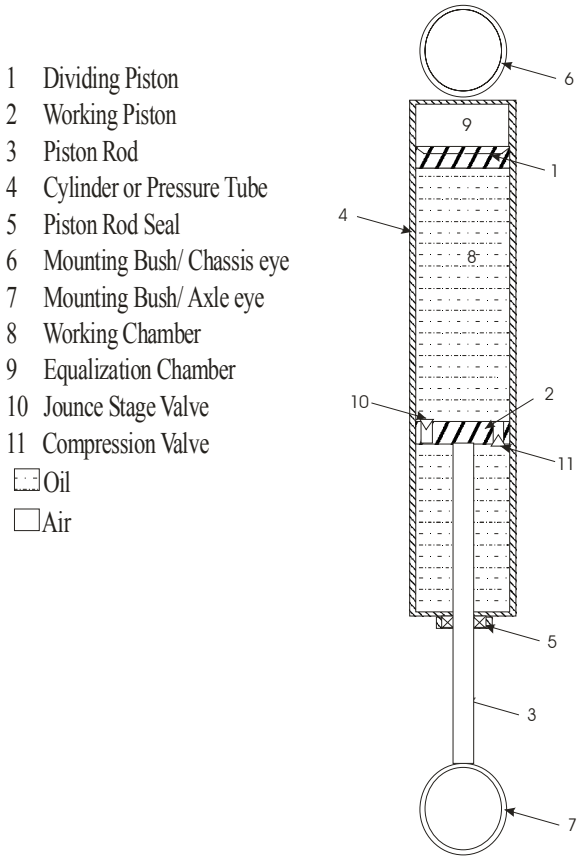


Fig. 2.2. Diagram of the single–tube shock absorber [1].

When the wheel jounces, the oil flows through the jounce state valve 10 from the bottom to the top part of the working chamber 8. The gas pressures in the equalization chamber 9 forces the dividing piston 1 to follow, the equalization going out the reduction in volume. If the wheel goes into the travel bump, the compression valve 11 is charged, and the dividing piston 1 moves upwards through the oncoming rod volume. The entire piston surface is available for bump damping.

Because tube 4 is longer, it is difficult to apply this design to passenger cars. However, it is an original equipment of many imported and domestic passenger cars such as SUV and light truck applications. A free–floating dividing piston 1 travels in the lower end of the pressure tube, separating the gas and the oil.

The difference in actual application is that in a single-tube design, the dividing piston 1 makes it possible to install the shock absorber in any position; it can be mounted upside down or right side up and will work either way. In this kind of shock absorber, the entire control during compression and extension takes place at the piston.

## 2.3 Comparison of Two Shock Absorbers

### 2.3.1 Twin-Tube Shock Absorber

The advantages and disadvantages of the twin-tube shock absorber are:

- Advantages:
  - Allows ride engineers to move beyond simple velocity sensitive on the valves and to use the position of the piston to fine tune the ride characteristic.
  - Adjusts more rapidly to changing road and weight conditions than single-tube shock absorbers.
  - A control is enhanced without sacrificing driver comfort. Two shocks absorbers into one -- comfort and control.
- Disadvantages:
  - Can only be mounted in one direction.
- Current Uses:
  - Original equipment on many domestic passenger cars, SUV and light truck applications.

### 2.3.2 Single-Tube Shock Absorber

The advantages and disadvantages of the single-tube designs are:

- Advantages:
  - Easy to tailor to specific applications, as the larger piston diameter allows low working pressures.
  - Sufficient room for valves and passages.
  - Can be installed in any position, can be mounted upside down, reducing the unsprung weight.
  - May run cooler. Heat is dissipated directly via the outer tube because it is exposed to the air.
- Disadvantages:
  - Longer than twin-tube shock absorbers.
  - The outer tube, which acts as a guide cylinder for the piston, is susceptible to damage from stone throw, etc. A dent in the pressure tube will destroy the unit.
  - Suspension layout must provide sufficient room for the tube which, with its very close tolerances, is not to be mechanically impeded in any way. This is a disadvantage when lines must be routed around the shock absorber in restricted bodywork areas.
  - The piston rod seal is subjected to the damping pressure.
  - Difficult to apply to passenger cars designed OE with twin-tube designs.
- Current Uses:
  - Original equipment for many import and domestic passenger cars, SUV and light truck applications.
  - Available for many after market applications.

### 2.3.3 Main Dimensions and General Characteristics of Two Types of Shock Absorbers

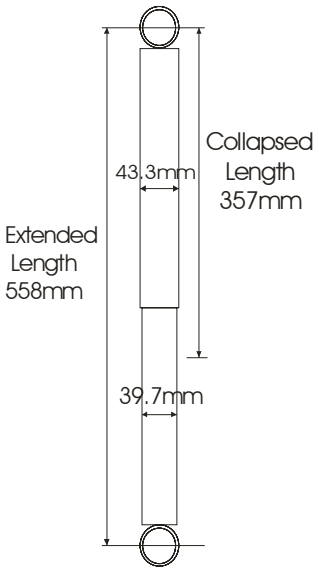


Fig. 2.3. Main dimensions of twin–tube shock design (an example).

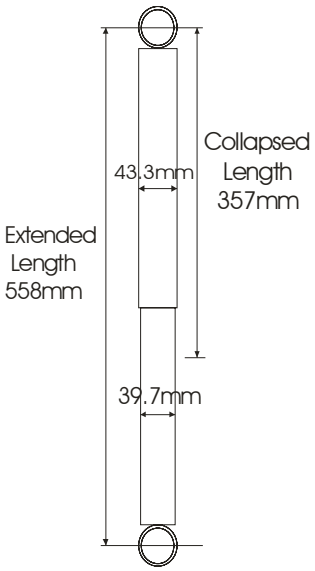


Fig. 2.4. Main dimensions of single–tube design (an example).

Table 2.1 Main Dimensions and General Characteristics of Two Types of Shock Absorbers

| TWIN-TUBE SHOCK ABSORBER | SINGLE-TUBE SHOCK ABSORBER |
|---|---|
| ▪ The length of the collapsed shock absorbers is between 280mm to 357mm and extended between 378mm to 558mm. | ▪ The length is greater than the length of the twin tube because due to the equalization chamber is located above the working chamber. It has sufficient room for valves and passages. |
| ▪ The working piston has a diameter of 24.4mm for a small bore, 28.3 for a medium bore, and 39.7mm for a large bore. | ▪ The working piston usually has a diameter of 30, 36, 45, or 46 mm, reducing the operating pressures. The piston rods have an 11 mm diameter. That is easy to tailor to specific applications because the larger piston diameter is possible to reduce the operating pressures. |
| ▪ In contrast to the single–tube shock absorber, mechanical measures can be taken at the outer cylinder to permit the routing of lines in restricted bodywork areas. | ▪ Suspension layout must provide sufficient room for the tube, which is not to be mechanically impeded in any way. This is a disadvantage when lines must be routed around the shock absorber in restricted bodywork areas. |
| ▪ Only specific installation positions are possible, so it is sensitive to overloading (damping ceases). | ▪ Can be installed in any position. If it is mounted upside down, reducing the unsprung weight. |
| ▪ Insensitive to external damage, and more sensitive valve response at small amplitudes. Remain functional even after loss of gas. | ▪ The outer tube, which acts as guide cylinder for the piston, is susceptible to damage from stone throw, etc. A dent in the pressure tube will destroy the unit. On the other hand, since the working tube is exposed to the air, it may run cooler. |

## 2.4 Performance Characteristics

The performance of shock absorbers can be described using force-speed characteristics that are shown in Fig. 2.5. The right side characteristics show graphically how the damping force exerted on the piston of the shock absorber depends on the (maximum) speed of the piston. The left side characteristics show the damping force developed at a particular position of the piston for the operation at the particular value of the stroke.

For example, at particular road conditions the piston is moving in one direction through the distance equal to the stroke. In the middle of the stroke, the piston is moving with the maximum speed, and at this speed the maximum force is exerted on it. When the piston moves in the opposite direction (negative value of speed), the negative force exerts the piston and the shape of the characteristic differs from that at positive speed.

The damping force of a shock absorber depends on the speed at which the two fixing points are pulled or pushed together. The damping force-speed curve can be progressive, linear or degressive, as is shown in Fig. 2.5. The curve shape (left side) and diagram (right side) are directly related. The smallest area and therefore the lowest mean damping, is in the diagram of the progressive curve, i.e. the actual mean damping, which is important for the springing behavior, is low. The largest area is that of the degressive curve with a rounded shape, and so it has a high mean damping.

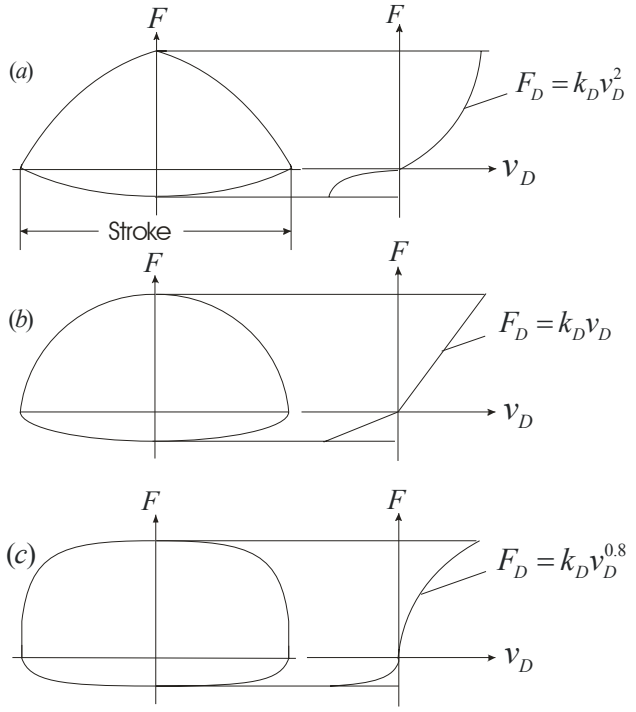


Fig. 2.5. Damping Force-Speed curves: a) progressive, b) linear, c) degressive [1].

The exponent $n$ can express the shape of the damping force curve $F_D$. In general, the force-speed characteristics can be described by the equation:

$$F_D = k_D v_D^n \tag{2.1}$$

where: for $n > 1$ - progressive curve
for $n = 1$ - linear curve
for $n < 1$ - degressive curve
$v_D$ - piston speed in $m/s$.
The mean piston speed $v_{D,mean}$ is:

$$v_{D,mean} = v_{D,\max} / 1.62 \tag{2.2}$$

As an example, Fig. 2.6. shows a degressive curve of the rear axle damping of a front-wheel drive vehicle. The maximum jounce force of 1.45 kN occurs at $v_{D,\max} = 0.52\ m/s$. However, piston speeds of $3\ m/s$ can occur, which leads to higher forces.

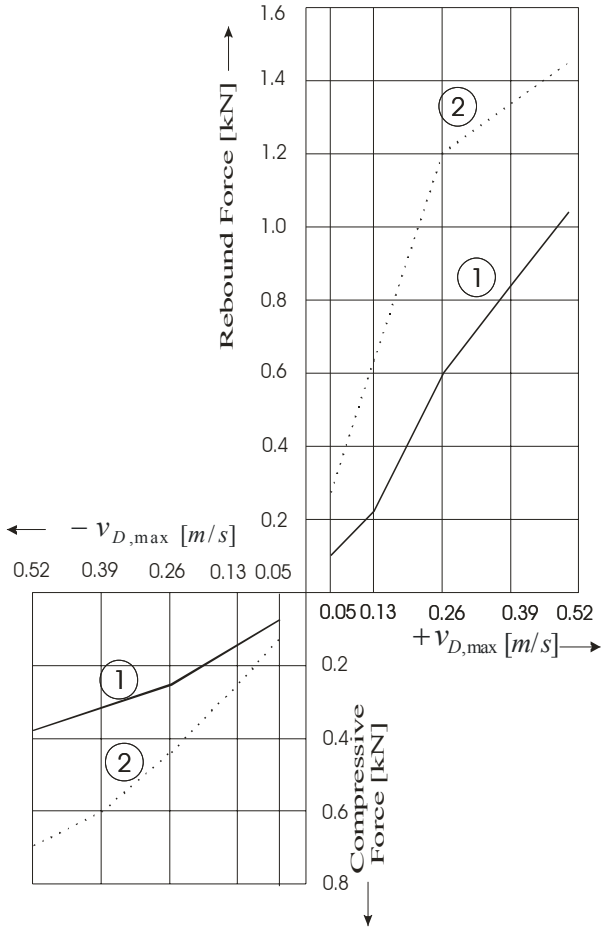


Fig. 2.6. Rear axle damping curve: 1 is the standard setting, and 2 is for the heavy-duty version [1].

# CHAPTER 3
# ELECTRIC SHOCK ABSORBER: GENERAL DESCRIPTION

## 3.1 Construction and Principle of Operation

The electric shock absorber converts the kinetic energy into electric energy. This energy can be used to charge the battery and to improve drive efficiency. The electric shock absorber is shown schematically in Fig. 3.1. It consists of a permanent magnet linear synchronous generator, a spring, and an electric energy accumulator [3].

The linear generator consists of two parts:

- Primary part with three-phase winding placed in the slots of primary core, and
- Secondary part with permanent magnets attached to the iron core.

The electric energy accumulator consists of a controlled rectifier and a battery connected to it.

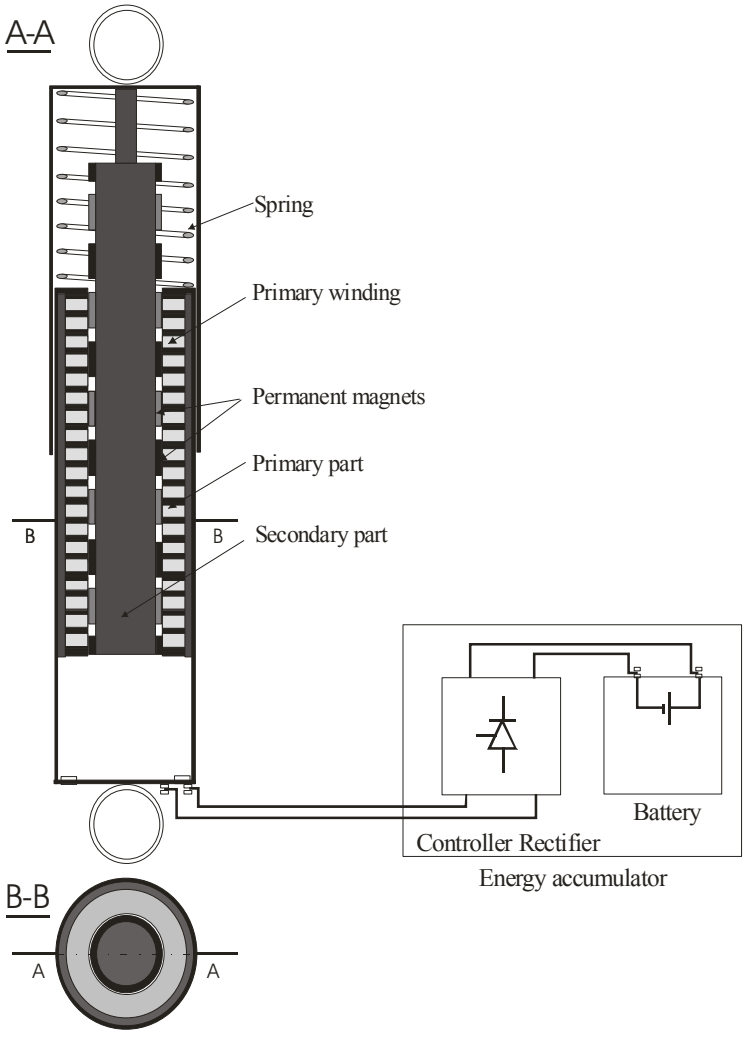


Fig. 3.1. Diagram of electric shock absorber: A-A – axial (longitudinal) crossection, B-B – perpendicular crossection.

During the oscillation of the vehicle, the secondary part is moving with respect to the primary part. Due to the relative linear motion of primary winding and secondary permanent magnets, an AC voltage is induced in the coils. This voltage is then rectified by the 3-phase controlled converter and supplies a battery.

Since the magnetic field produced by the permanent magnets alternates with respect to the primary part, the core of this part must be laminated to decrease the eddy current losses and hysteresis losses. The secondary core can be made of solid iron since the magnetic flux is steady in it.

### 3.2 Presentation of Several Designs of Linear Generator

Considering the topology of LSM, one of the parts has to be shorter than another in order to ensure the unchangeable active length of the machine. Since the longer primary part makes the machine heavier and more costly, a LSM with a short primary part will be considered only.

In this chapter, several designs are presented. The cross-sectional views of the Permanent Magnet Linear Synchronous Generators (PMLSG) are shown in Figs. 3.2. and 3.3.

Regarding a mutual position of primary and secondary parts, two groups of LSMs can be specified:

- machines with external primary part (internal secondary part): types I, II and III (Figs. 3.2.a., 3.2.b. and 3.2.c.).
- machines with internal primary part (external secondary part): types IV, and V (Figs. 3.3.a., and 3.3.b.).

With regard to primary structure, two groups of LSMs can be distinguished:

- machines with coils placed in the slots: types I, II and IV (Figs. 3.2.a., 3.2.b. and 3.3.a.).
- machines with slotless winding: types III, and V (Figs. 3.2.c. and 3.3.b.).

Taking into account the structure of a secondary part, two designs of LSMs can be mentioned:

- machines with secondary part with buried permanent magnets: types I, and III: (Figs. 3.2.a. and 3.2.c.).
- machines with secondary part with surface mounted permanent magnets: types II, IV and V (Figs. 3.2.b., 3.3.a. and 3.3.b.).

In tubular structures of LSM the laminations of the primary core may be either longitudinal or disk-shaped as in linear induction machines. Stacking of the disk laminations increases the effective airgap. The core of the secondary of a tubular PMLSM is generally made of solid magnetic steel. The polyphase three-phase armature winding can be distributed in slots or made as coreless (air cored) winding layers.

The linear generator can have the primary part outside, while the secondary part is inside (ferromagnetic cylinder with the inner or outer permanent magnets), or in another version it has the primary part inside, while the secondary part is placed outside surrounding the winding.

The linear generator of Type I (Fig. 3.2.a) has the shorter primary part outside, with a slotted three-phase armature winding. The secondary part is longer and placed inside, and it is a ferromagnetic cylinder with the buried permanent magnets.

Type II (Fig. 3.2.b) is similar to Type I, with the shorter primary part placed outside, and the longer secondary part placed inside. The primary core is slotted. This version has outer permanent magnets.

Type III (Fig. 3.2.c) is similar to Type I. The primary part is shorter and placed outside, while the secondary part is longer and placed inside, and with buried magnets. The primary in this version is slotless.

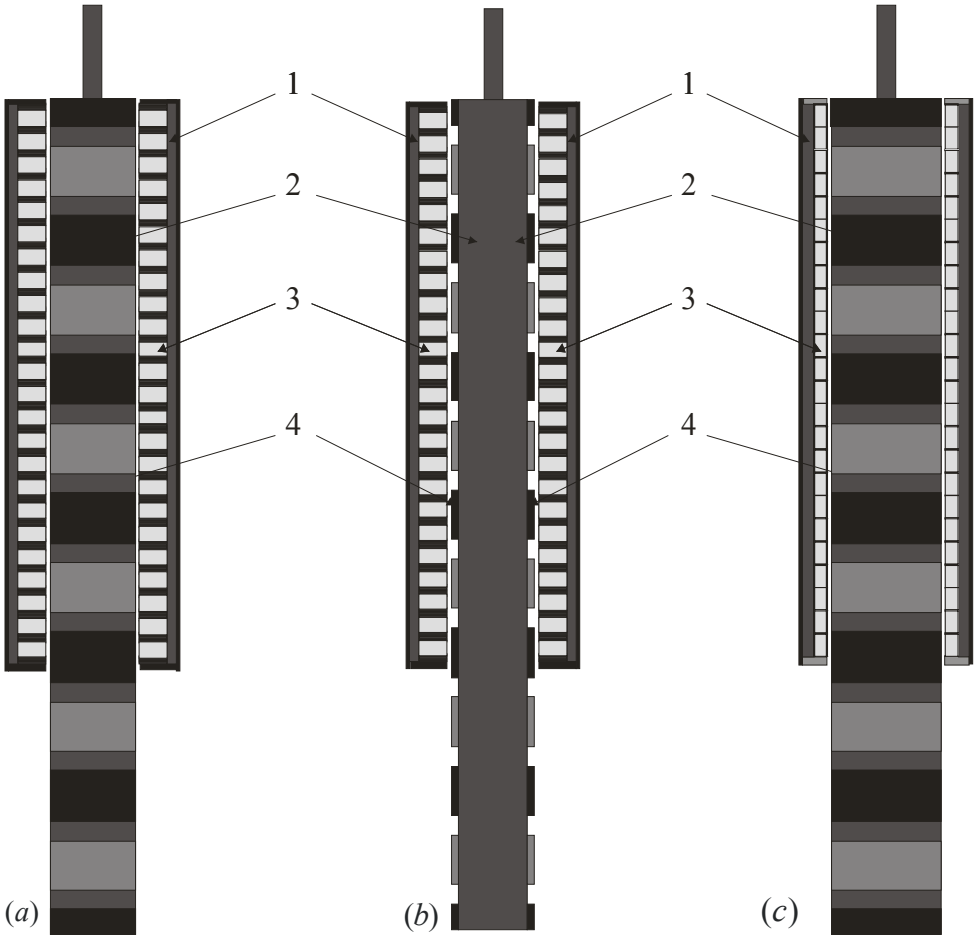


Fig. 3.2. Permanent magnet linear generators with outer primary part: 1- Primary part, 2- Secondary part, 3- Primary winding, 4- Permanent magnets.
(a) Type I – primary winding placed in the slots, secondary with buried magnets, (b) Type II – primary winding in the slots, secondary with surface mounted magnets, and (c) Type III – slotless primary winding, secondary with buried magnets.

Type IV (Fig. 3.3.a) has the primary winding placed in the slots with the outer secondary part with surface mounted magnets.

Type V (Fig. 3.3.b) is similar to Type IV. The only difference is that it has slotless winding.

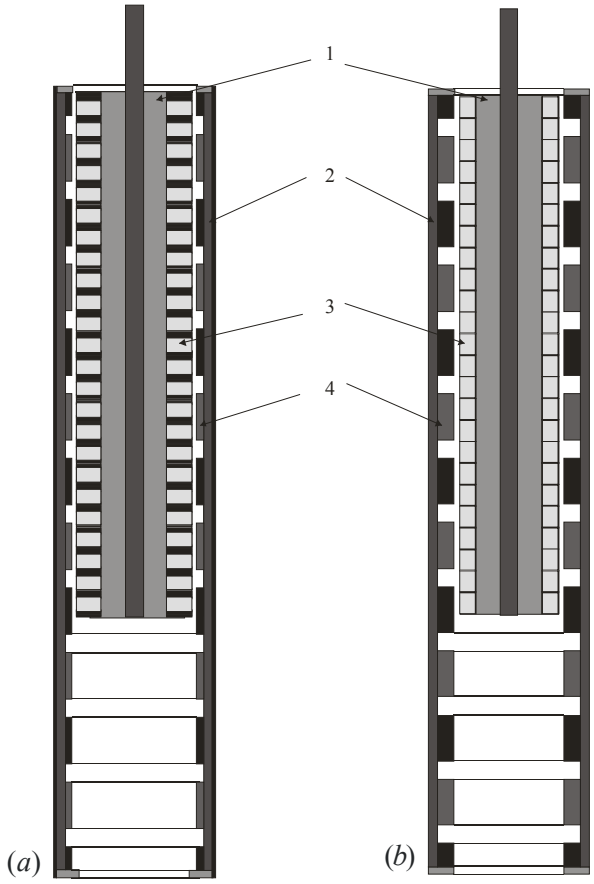


Fig. 3.3. Permanent magnet linear generators with inner primary part: 1- Primary part, 2- Secondary part, 3- Primary winding, 4- Permanent magnets.
(a) Type IV – primary with winding in the slots, secondary with surface mounted magnets, (b) Type V – slotless primary winding, secondary with surface mounted magnets.

### 3.3 Qualitative Assessment and Selection of a Design for Further Study

In an electrical shock absorber, one part of LSM must be stationary while the other part is then moving (runner). In general, either the primary part or the secondary part can be stationary. In the LSM with the wound-coil runner (types IV and V) must have appropriate means for supplying it electrically. The disadvantage of the secondary as a runner (types I, II and III) is that the permanent magnets are exposed to continuous vibrations, which may demagnetize the magnets. For all these reasons, permanent magnet rotors are advantageous over wound-coil rotors.

It is preferable to have the secondary longer than the primary (all types) because having a smaller primary, the coil windings can be kept at a minimum relative to the active area. It is a trade off between maximizing the active area and keeping the cost of the secondary down. The longer a primary part, the higher is the power loss.

In types I, II and III, the outer cylinder forms the primary core. If the winding is in the toothed primary core, and located in open slots (types I and II), the effective airgap becomes considerably greater than the actual airgap. Slotless PMLSMs (types III and V) are detent force free motors, and provide lower torque ripple than slotted LSMs (types I, II and IV). On the other hand, a larger non-ferromagnetic airgap requires more PM material; the flux density is lower than that of slotted motors, and the current is higher. The magnetic flux density in the air gap of the slotted generator is stronger, which allows higher voltage to be generated at the same oscillation motion; consequently, more energy is sent to the battery, which means the damping coefficient in this version (types I, II and IV) can be higher.

The LSM of types I and III have buried magnets, while types II, IV, and V have surface magnets. The latter group has a bigger airgap, and the armature reaction is smaller.

For adequate clearance the airgap in all cases usually has to be substantially wider than in a conventional rotary machine.

For all the reasons mentioned before, the best option for the electric shock absorber seems to be type II (Fig. 3.2.b). This model of the electric shock absorber will be used for further study. LSM of type II is a generator with the shorter external primary part; the coils are placed in the slots, and the secondary part has surface mounted permanent magnets.

# CHAPTER 4
# DESIGN OF PERMANENT MAGNET LINEAR SYNCHRONOUS GENERATOR AND SPRING

A linear generator can be excited either by the field winding or by permanent magnets. In the case of a linear generator with permanent magnets, its operation conditions depend not only on permanent magnets, but also on the entire magnetic circuit. They also depend on how the magnets are installed and if the circuit is magnetized before of after the installation. It is fundamental to determine the size of the magnets. First, it is necessary to choose a specific type of permanent magnet, because each kind of magnet has a unique characteristic.

## 4.1 Permanent Magnet Characteristics

### 4.1.1 Demagnetization Curve and Magnetization Parameters

A permanent magnet can be described by its B-H curve which usually has a wide hysteresis loop (Fig. 4.1.). For permanent magnets, the essential part of the B-H curve is the second quadrant, called the demagnetization curve. There are two significant points on this curve: one at $H = 0$, where the magnetic flux density is equal to Br (remanent magnetic flux density, or remanence), another point $H_c$ at point $B = 0$, where a reverse magnetic field intensity is applied to a magnetized permanent magnet (coercive force, or coercitivity).

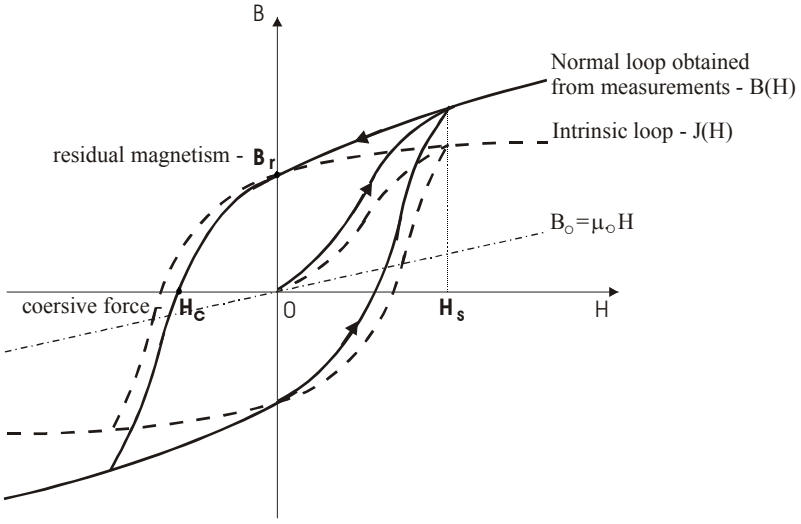


Fig. 4.1.Normal and intrinsic hysteresis loops of a permanent magnet material [16]

The saturation magnetic flux density $B_{sat}$ corresponds to high values of magnetic field intensity when an increase in the applied magnetic field produces no further significant effect on the magnetic flux density.

Maximum magnetic energy per unit produced by a PM is the maximum energy density per volume:

$$W_{\max} = \frac{(BH)_{\max}}{2} \ [J/m^3] \tag{4.1}$$

In electric machines technology, the following PM materials are used (see Fig. 4.2. and Table 4.1.):

- Alnico (Al, Ni, Co, Fe);
- Ferrites (ceramics), e.g., barium ferrite $BaO \times 6Fe_2O_3$ and strontium ferrite $SrO \times 6Fe_2O_3$;
- Rare-earth materials, i.e., samarium-cobalt $SmCo$ and neodymium-iron-boron $Nd - Fe - B$

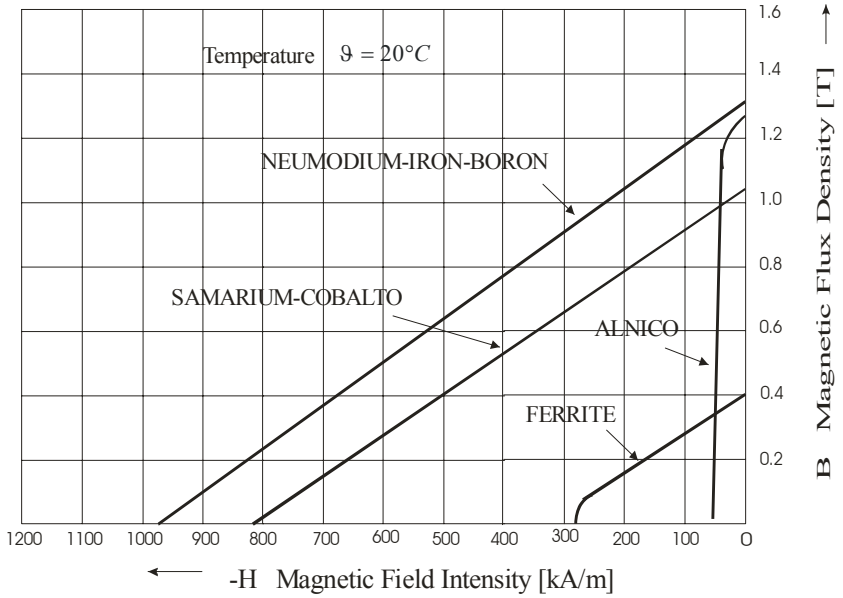


Fig. 4.2. Demagnetization curves for different permanent magnet materials [12].

Alnico magnets were used by the PM machines industry from the mid 1940s to about 1970. They have high magnetic remanent flux and low temperature coefficients, but low coercive force and the extremely non-linear demagnetization curve.

In the 1950s, Ferrites were invented. They have a higher coercive force than that of Alnico, but they have a lower remanent magnetic flux density. They have a low cost and very high electric resistance, not having eddy-current losses in the PM volume.

Rare earths PMs have been developed during the last three decades having great progress concerning available energy density. The first generation of the rare earths PMs are based on the composition $SmCo_5$, with a high remanent flux density, high coercive force, high-energy product, linear demagnetization curve, and low temperature coefficient. The only disadvantage is the high cost, due to the supply restriction of $Sm$ and $Co$.

Based on the cost, a second generation of rare earth has been discovered with neodymium $Nd$ and iron. The $Nd$ is much more abundant than $Sm$. $Nd-Fe-B$ magnets have better properties than $SmCo_5$, but unfortunately the disadvantage is that their demagnetization curves depend on the temperature, and are also susceptible to corrosion. Protection of $Nd-Fe-B$ magnets for metallic ($Sn$ or $Ni$) or organic (electro-painting) is the best method of protection against corrosion [12].

Table 4.1. Parameters of permanent magnet materials [16].

| Material | $(B\cdot H)_{\max}$ $[kJ/m^3]$ | $B_r$ $[T]$ | $H_c$ $[kA/m]$ |
|---|---|---|---|
| Ceramics | 27 – 35 | 0.4 | 240 |
| Alnico | 70 - 85 | 1.1 | 130 |
| Rare earth magnets: | | | |
| - $SmCo_5$ | 160 - 200 | 0.9 – 1.0 | 660 - 750 |
| - $Sm_2Co_{17}$ | 205 - 240 | 1.04 – 1.12 | 760 - 820 |
| - $Nd-Fe-B$ | 190 - 385 | 1.0 – 1.4 | 760 - 980 |

If the temperature increases, there is some degradation of the properties of the permanent magnets, and they vanish completely at Curie temperature. Table 4.2. shows these changes. Coefficients $C_C$ and $C_B$ show in percents the reversible changes in remanence and coercive force.

Table 4.2. Temperature influence on permanent magnet materials [16].

| Material | Temperature Curie $[°C]$ | Max. Operat. Temp.$[°C]$ | $C_B$ $[\%/K]$ | $C_C$ $[\%/K]$ |
|---|---|---|---|---|
| Ceramics | 450 | 300 | -0.20 | +0.40 |
| Alnico | 830 | 500 | -0.02 | +0.01 |
| Rare earth magnets: | | | | |
| - $SmCo_5$ | 720 | 250 | -0.045 | -0.25 |
| - $Sm_2Co_{17}$ | 800 | 300 - 350 | -0.045 | -0.25 |
| - $Nd-Fe-B$ | 310 | 210 - 100 | -0.13 | -0.60 |

The material recommended for the model in this project is the $Nd-Fe-B$ since it considerably improves the performance-to-cost ratio. Ferrites are not used because they would increase the size of the shock absorbers, and $SmCo_5$ would increase the cost.

Fig. 4.3. shows the characteristics of demagnetization of VACODYM 383, a material produced by German Company Vacuumschmelze. There are two types of characteristics $B(H)$ and $J(H)$ for different temperatures. Magnetic flux density is shown in $tesla(T)$ and $kilo-gaus(kG)$ and field strength in $KA/m$ and $kilo-oesteads(kOe)$.

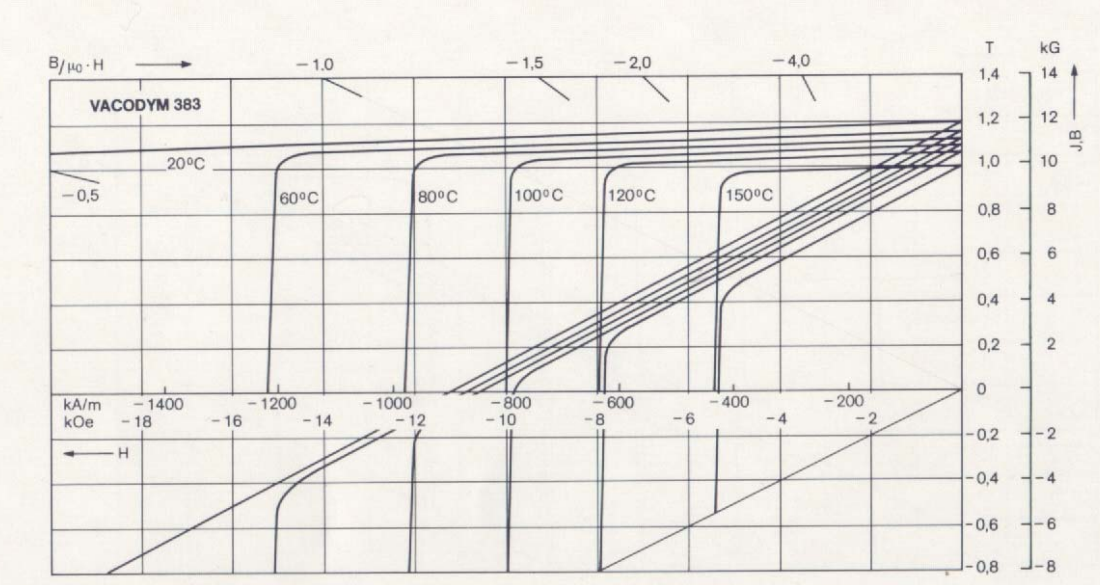


Fig. 4.3. Demagnetized characteristics of VACODYM 383, material produced by German Company Vacuumschmelze [22]

### 4.1.2 Determination of the Operating Point of the Permanent Magnets

If $B$ is the magnetic flux density, the total magnetic flux $\phi$ can be expressed as

$$\phi = \int_A B.dA \tag{4.2}$$

where the integral is over an area $A$. So, if the magnetic flux density through the transversal section of a core is uniform:

$$\phi = BA \tag{4.3}$$

where: $\phi$ - core flux
$B$ - flux density in the core
$A$ - transversal section area of a core

The relation between the magnetomotive force (mmf), and the magnetic field intensity for magnetic circuits is given by

$$mmf = Hl \tag{4.4}$$

where: $H$ - average magnitude of field intensity in the core
$l$ - average length of the core

The relation between the magnetic field intensity $H$ and the magnetic density $B$ depends on the material in which the field exists, and

$$B = \mu H \tag{4.5}$$

where: $\mu$ - magnetic permeability.

To determine the dimensions of the permanent magnet, let assume that the magnetic core permeability $\mu_{Fe} = \infty$. Thus, the whole magnetic voltage drop is in the airgap. If the Ampere's law is applied to a closed magnetic circuit, which consists of a magnetic core of $\mu = \infty$, then the magnet of length $l_m$, and an air-gap of length $g$ (Fig. 4.4.):

$$H_m l_m + H_g g = 0 \tag{4.6}$$

where: $H_m, H_g$ - are the field intensities in the magnet and in the air-gap

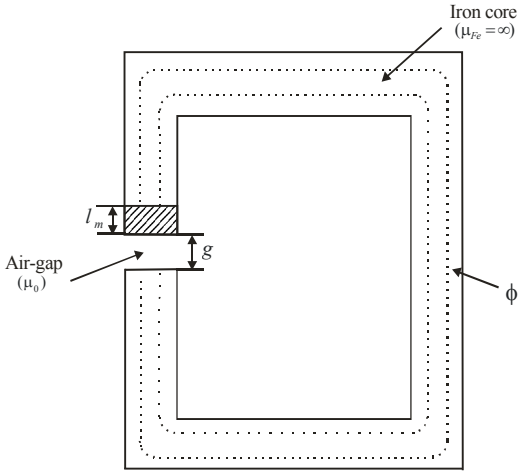


Fig. 4.4. Magnetic circuit with permanent magnet.

Since the flux must be continuous in the magnetic circuit

$$\phi = A_g B_g = A_m B_m \tag{4.7}$$

for the air-gap

$$B = \mu_0 H_g \tag{4.8}$$

after substitution of (4.8) to (4.6)

$$B = -\frac{l_m}{g} \mu_0 H_m \tag{4.9}$$

The above equations are shown using characteristics in Fig. 4.5. The intersection of two characteristics, where the flux density in the magnet and in the airgap is the same ( $B(H_m) = B_g(H_g)$ ), determines the operating point $P$.

From equation (4.9) the ratio is

$$\frac{l_m}{g} = -\frac{B}{\mu_0 H_m} \tag{4.10}$$

and it is marked in Fig. 4.3.

The equation for the rectilinear magnetization characteristic

$$B = B_r\left(1 - \frac{H}{H_0}\right) \tag{4.11}$$

and, after transformation

$$H = \frac{H_0(B_r - B)}{B_r} \tag{4.12}$$

On the basis of equations (4.12) and (4.9), the expression is obtained to determine the flux density in the point $P$:

$$B_P = \frac{l_m \mu_0 H_0 B_r}{g B_r - l_m \mu_0 H_0} \tag{4.13}$$

From equations (4.11) and (4.9), the equation for the calculation of flux intensity in the point $P$

$$H_P = -\frac{g B_r H_0}{g B_r - l_m \mu_0 H_0} \tag{4.14}$$

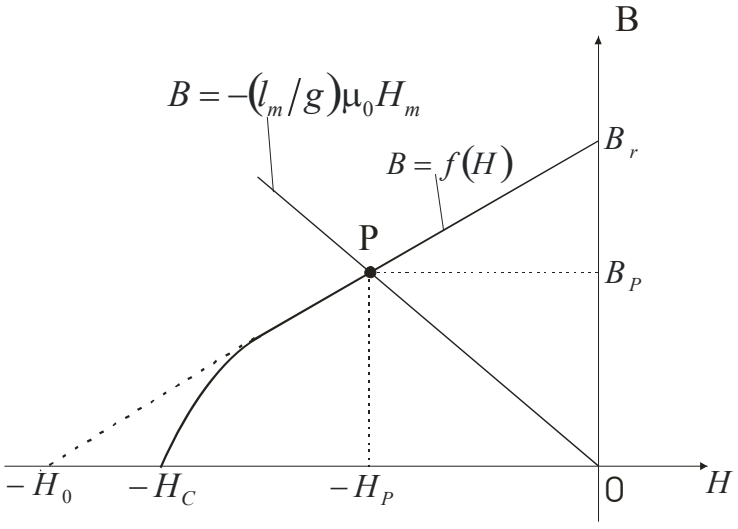


Fig. 4.5. Determination of the operating point of the permanent magnet [16].

## 4.2 Design of Linear Generator

### 4.2.1 Dimensions of Stator and Rotor Cores

The linear generator is excited by permanent magnets attached to the secondary ferromagnetic core that can be made of solid iron. The iron core is rigidly attached to the outer cylinder, which is also made of the solid iron. Another part of the generator (primary part) is attached to the bottom cover (Fig 3.1.). During the oscillation the magnets are moving with respect to the winding, inducing in it an ac voltage.

To determine the dimensions of the magnetic circuit, only a section of the generator equal to the length of pole pitch is considered (Fig. 4.6.)

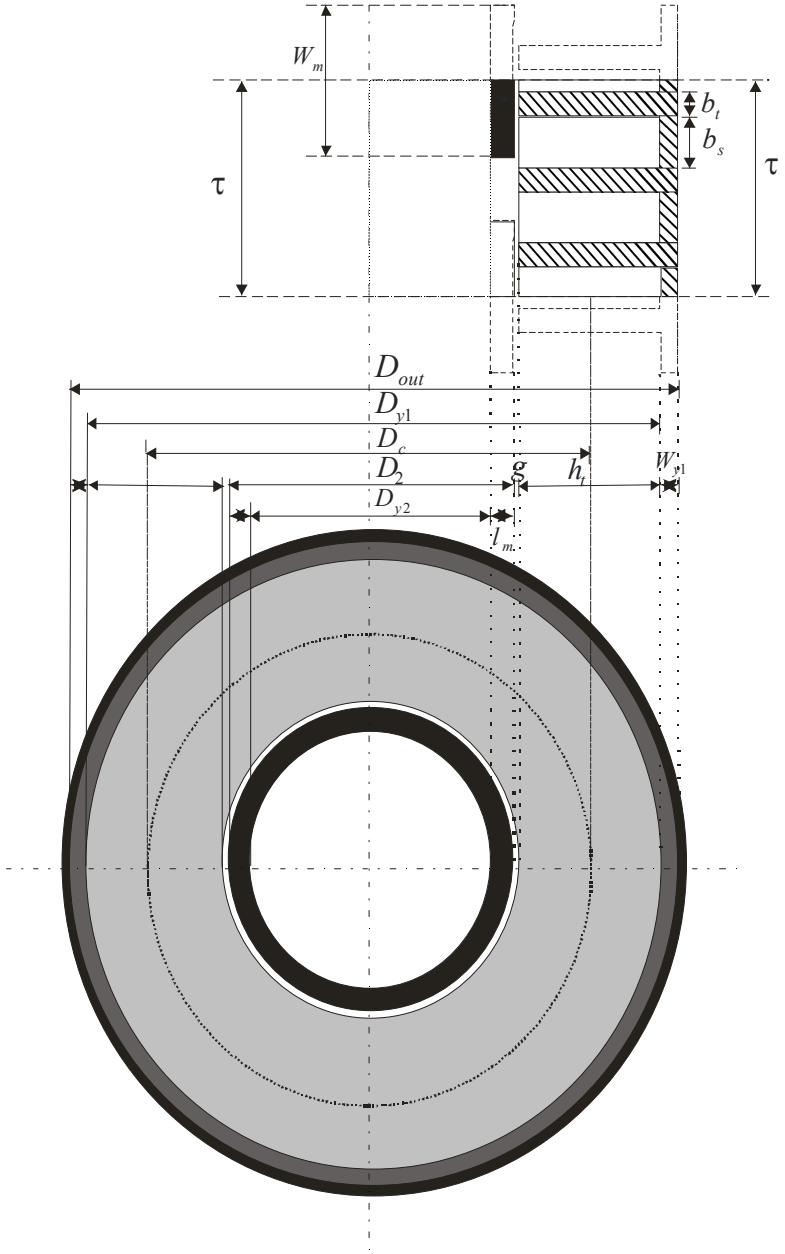


Fig. 4.6. Transversal section of the PMLSG.

If the pole pitch $\tau$ of the generator is given, the magnet width

$$W_m = K_m \tau \tag{4.15}$$

where $K_m = 0.65 - 0.75$
the tooth pitch:

$$\tau_t = \frac{\tau}{qm} \tag{4.16}$$

where: $m$ - number of phases
$q$ - number of slots per pole per phase

To determine the tooth width, it is assumed that the entire magnetic flux crossing the air-gap is in the teeth. That means:

$$\phi = B_g A_g = B_t A_t \tag{4.17}$$

where: $B_g$ - magnetic flux density in the air-gap
$B_t$ - magnetic flux density in the teeth
$A_g$ - crossection area on the magnet surface along a half pole-pitch

$$A_g = \pi D_2 \left( \frac{W_m}{2} \right) \tag{4.18}$$

$D_2$ - outer diameter for the secondary (Fig. 4.6.)
$A_t$ - The cross-section area in the tooth

$$A_t = (\pi D_2 b_t) K_{Fe} \tag{4.19}$$

$K_{Fe}$ - iron density in the tooth
$b_t$ - tooth width

By substitution of (4.18) and (4.19) in (4.17), the tooth width

$$b_t = \left( \frac{1}{K_{Fe}} \right) W_m \frac{B_g}{2B_t} \tag{4.20}$$

and the slot opening is calculated as the difference

$$b_s = \tau_t - b_t \tag{4.21}$$

Due to the primary part slots, the magnet flux experiences an increase of the real air-gap. Thus the new equivalent air-gap

$$g_{eq} = K_c g \tag{4.22}$$

where the Carter's coefficient $K_c$ [6]

$$K_c = \frac{\tau_t (5g + b_s)}{\tau_t (5g + b_s) - b_s^2} \tag{4.23}$$

The thickness of the permanent magnet $l_m$ is determined from the B-H characteristic for a particular type of magnet and from the length of the airgap (Fig. 4.5.). From Eqns. 4.9 and 4.12

$$l_m = \frac{g_{eq} B_r B_g}{\mu_0 H_c (B_r - B_g)} \tag{4.24}$$

To determine the magnetic flux density, it is assumed that the same magnetic flux, which is in the air-gap, is also in the secondary core. Thus:

$$\phi = B_g A_g = B_{y2} A_{y2} \tag{4.25}$$

where: $B_{y2}$ - the flux density in secondary core

$$B_{y2} = B_g \left( \frac{A_g}{A_{y2}} \right) \tag{4.26}$$

$A_{y2}$ - crossection area of the surface for magnetic flux in secondary yoke

$$A_{y2} = \pi \left( \frac{D_{y2}}{2} \right)^2 \tag{4.27}$$

$D_{y2}$ - diameter of the secondary core (Fig. 4.6.)

$$D_{y2} = D_2 - 2l_m \tag{4.28}$$

To determine the magnetic flux density on the primary surface, it is assumed that the same magnetic flux, which is in the air-gap, is also in the primary part. Thus:

$$\phi = B_g A_g = B_{w1} A_{w1} \tag{4.29}$$

where: $B_{w1}$ - flux density on the surface of the primary part

$$B_{w1} = B_g \left( \frac{A_g}{A_{w1}} \right) \tag{4.30}$$

$A_{w1}$ - crossection area of the surface for half of the magnetic flux on the primary surface

$$A_{w1} = \pi \left( D_2 + 2g_{eq} \right) \left( \frac{W_m}{2} \right) \tag{4.31}$$

### 4.2.2 Parameters of Primary Winding

The winding parameters depend on the voltage of the accumulator and on the damping force that the generator ought to perform. In order to transmit the power from the generator to the battery, the line emf $E$, induced in the winding, must be greater than the voltage of the accumulator $V_a$ (Fig. 4.7.).

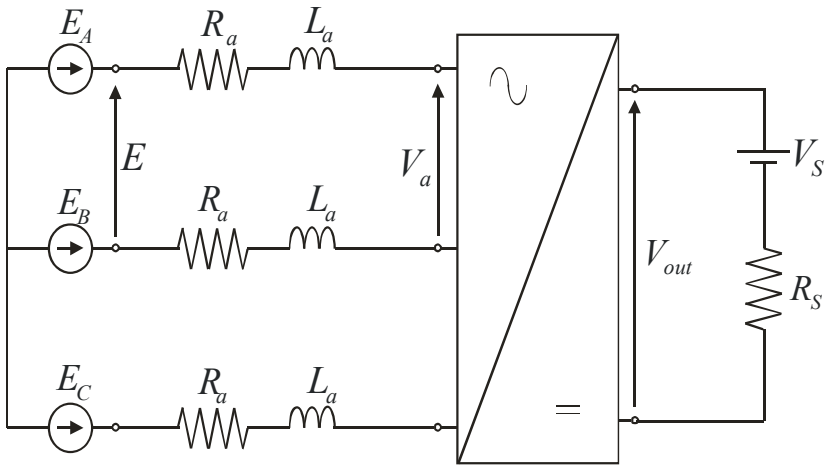


Fig. 4.7. Circuit of electric shock absorber.

The phase electromotive force is proportional to the linear speed

$$E_\phi = K_E v \tag{4.32}$$

where the generator constant

$$K_E = 2N_c B_{w1} l_t pq \tag{4.33}$$

and then the number of turns in the coil

$$N_c = \frac{E_\phi}{2B_{w1} l_t pqv} \tag{4.34}$$

where: $B_{w1}$ - flux density on the primary surface (Eqn. 4.30)

$l_t$ - length of the coil turn on the smooth surface of the equivalent stator core:

$$l_t = \pi\left(D_2 + 2g_{eq}\right) \tag{4.35}$$

$p$ - number of pole-pairs

$q$ - number of slots per pole per phase

$v$ - secondary speed

The number of turns per phase

$$N_p = 2N_c pq \tag{4.36}$$

The average value of line-to-line electromotive force (Fig. 4.8.)

$$E = \frac{3\sqrt{3}}{\pi} E_\phi \tag{4.37}$$

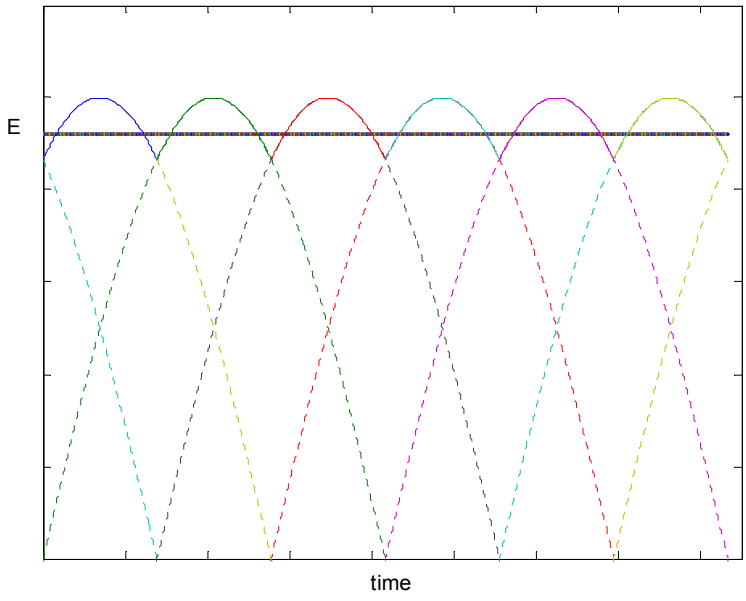


Fig. 4.8. Line to line voltages and output voltage in a three-phase rectifier.

For the purpose of the design calculations, the simplified equivalent circuit of LSM is used (Fig. 4.9). The machine seen from the output terminals of rectifier (see Fig. 4.7) reminds the DC generator with commutator (mechanical rectifier). Assuming

a little change of the output DC current $I$ and ignoring the voltage drop across the motor inductance, the output voltage at steady state conditions

$$V_{out} = E - 2\left(R_\phi I\right) \tag{4.38}$$

where $R_\phi$ is the phase resistance.

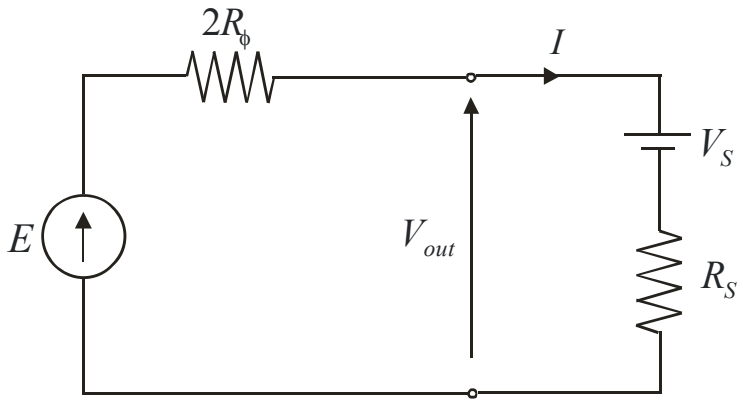


Fig. 4.9. Simplified equivalent circuit of the electric shock absorber.

The electromotive force can be expressed as an increase of the output voltage

$$E = K_e V_{out} \tag{4.39}$$

where $K_e \geq 1$ is the emf coefficient, and it should be corrected after calculation.

A maximum phase electromotive force

$$E_\phi = K_e \frac{\pi}{3\sqrt{3}} V_{out} \tag{4.40}$$

The rms value of the phase current

$$I_\phi = \sqrt{\frac{2}{3}} \times I \tag{4.41}$$

If the mechanical power loss is ignored, the average input power of the generator

$$P_{in} = Fv = EI \tag{4.42}$$

The force developed by the generator is obtained substituting (4.37), (4.32), and (4.33) in (4.42)

$$F = \frac{3\sqrt{3}}{\pi} 2 N_c B_{w1} l_t pqI \tag{4.43}$$

The crossection area of the wire depends on the rms value of the current $I_\phi$ and on the current density in the wire $J_{cu}$

$$A_w = \frac{I_\phi}{J_{cu}} \tag{4.44}$$

since the area $A_w = \pi\left(\frac{D_w}{2}\right)^2$, the wire diameter

$$D_w = 2\sqrt{\frac{A_w}{\pi}} \tag{4.45}$$

The current density in the wire $J_{cu}$ depends on the cooling conditions and the type of insulation: for poor ventilation $J_{cu} = (1-4)\ A/mm^2$, and for good ventilation $J_{cu} = (5-7)\ A/mm^2$.

The crossection area of the coil copper

$$A_{ccu} = N_c A_w \tag{4.46}$$

The crossection area of the coil (with insulation)

$$A_c = \left(\frac{A_{ccu}}{K_{cu}}\right) \tag{4.47}$$

where $K_{cu} = (0.4-0.7)$ is the coefficient of copper density in the coil.

The crossection area of the coil is $A_c = b_s h_t$ (see Fig. 4.6.), so the length of the tooth

$$h_t = \left(\frac{A_c}{b_s}\right) \tag{4.48}$$

The phase resistance $R_\phi$ of the conductive wire at ambient temperature is determined from the conductivity of the material $\sigma$, the length of the wire $l_\phi$, and the conductive area $A_w$

$$R_{\phi} = \frac{l_{\phi}}{\sigma A_w} \tag{4.49}$$

where: $l_{\phi}$ - length of the wire per phase

$$l_{\phi} = 2 l_c N_c pq \tag{4.50}$$

$l_c$ - average length of the coil

$$l_c = \pi \times D_c \tag{4.51}$$

$D_c$ - average coil diameter (Fig. 4.6.)

$$D_c = D_2 + 2 g_{eq} + h_t \tag{4.52}$$

The phase resistance needs to be adjusted to the operating temperature

$$R_{\phi T} = R_{\phi} \frac{T_c - \alpha_T}{T_a - \alpha_T} \tag{4.53}$$

where: $T_c$ - work temperature for the winding in Kelvine's degree

$T_a$ - wire base temperature in Kelvine's degree for resistance $R_{\phi}$

$\alpha_T$ - temperature coefficient, which: for copper $\alpha_T = 38K$ , and for aluminum $\alpha_T = 28K$

The phase inductance $L_a$ of the symmetrical generator with surface mounted permanent magnets

$$L_a = L_l + \frac{3}{2} L_m \tag{4.54}$$

where: $L_l$ - leakage inductance

$L_m$ - magnetizing inductance of a single phase

Since the gap (airgap + magnet thickness) is relatively high, the magnetizing inductance of the deep slot winding is smaller than of the slot leakage inductance. Thus, it is assumed that $L_a \cong L_l$ . The predominant component in the leakage inductance is the slot inductance, which is equal to (see Appendix A, [7]):

$$L_l = 2\pi \mu_0 N_c^2 D_c pq \frac{h_t}{6 b_s} \tag{4.55}$$

### 4.2.3 Dimensions of Primary Core

Having known the dimensions of the slots, the dimensions of the stator elements can be determined (see Fig. 4.6.).

It is assumed that the same magnetic flux, which is in the air-gap over one half of the magnet, is also in the stator yoke

$$\phi = B_g A_g = B_{y1} A_{y1} K_{Fe} \tag{4.56}$$

where: $B_{y1}$ - permissible flux density in the primary yoke

$A_{y1}$ - crossection area of the primary yoke

$$A_{y1} = K_{Fe} \pi D_{y1} W_{y1} \tag{4.57}$$

$D_{y1}$ - primary yoke diameter

$$D_{y1} = D_2 + 2(g + h_t) \tag{4.58}$$

By substitution of (4.18) and (4.57) in (4.56), the thickness of the primary yoke

$$W_{y1} = \frac{1}{K_{Fe}} \left( \frac{B_g}{B_{y1}} \right) \left( \frac{\frac{\pi D_2 W_m}{2}}{\pi D_{y1}} \right) \tag{4.59}$$

where $K_{Fe}$ is the iron density coefficient in the laminated core

The outer diameter of the primary

$$D_{out1} = D_{y1} + 2W_{y1} \tag{4.60}$$

### 4.2.4 Length of Primary and Secondary Parts

The length of the primary winding depends on the tooth pitch $\tau_t$, the numbers of turns per phase $N_p$, the numbers of turns per coil $N_c$, and the number of phases $m$

$$l_{prim} = \tau_t \left( \frac{N_p}{N_c} \right) m \tag{4.61}$$

The length of the active part of the secondary must be the same as the length of the primary. It depends on the pole pitch $\tau$ and on the number of the pair poles $p$

$$l_{\text{sec}(active)} = 2p\tau \tag{4.62}$$

Since the secondary part moves, and in order to have the same active part during the oscillation, the real length of the secondary must be greater than the primary. In this case, the secondary will have two more pair poles:

$$l_{\text{sec}} = 2(p+2)\tau \tag{4.63}$$

### 4.2.5 Voltage Drop

Referring to the simplified equivalent circuit of the generator shown in Fig. 4.9., the output voltage:

$$V_{out} = \frac{3\sqrt{3}}{\pi} E_{\phi} - 2\Delta V_R \tag{4.64}$$

and the voltage drop across the phase resistance $R_{\phi T}$

$$\Delta V_R = R_{\phi T} I \tag{4.65}$$

### 4.2.6 Power Losses

In a generator there are three kinds of losses:

a) core losses, due to the change of magnetic field; these losses take place in the stator steel, and they consist of the hysteresis losses and the losses due to the eddy currents.
b) copper losses; they are resistive losses in the coil windings
c) mechanical losses due to friction and ventilation.

The copper (resistive) losses, which are the only losses considered in this application, appear in the conductor with the electrical resistance $R_{\phi T}$ carrying a current $I$ :

$$\Delta P_C = 2R_{\phi T} I^2 \tag{4.66}$$

The output power

$$P_{out} \cong V_{out} I \tag{4.67}$$

and the generator efficiency:

$$\eta = \frac{P_{out}}{P_{in}} \cong \frac{P_{out}}{P_{out} + \Delta P_c} \tag{4.68}$$

## 4.3 Design of Spring

There are many different types of springs and spring materials. In the design calculations, the following assumptions are considered:

a) The type and form of the spring will be the compression spring ground.
b) The material must be chosen for the maximum energy and mass, such as music wire, ASTM A228, Chrome Vanadium or Chrome Silicon steel wire.
c) The ends of the spring are to be closed and ground.
d) The spring is to have maximum energy for the limited space, while the stress level is not to exceed the maximum yield strength of the wire.
e) The spring operates periodically with a long interval of rest.
f) If the spring requires the use of material 0.5" or larger in diameter, wound hot from bar stock will be used.

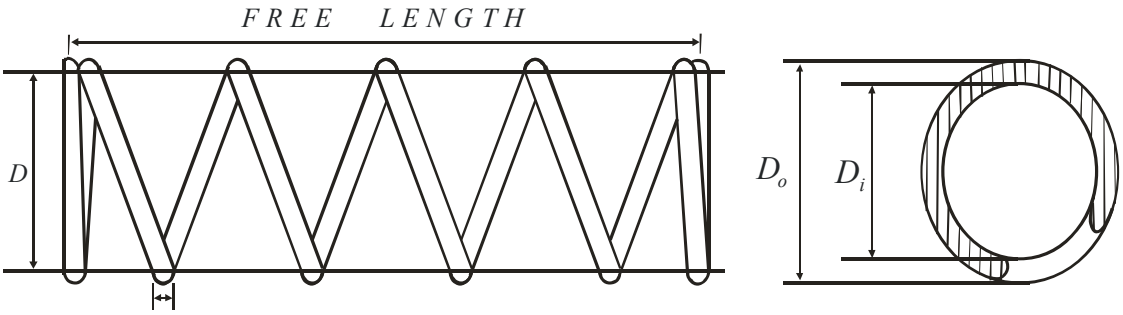


Fig. 4.10. Scheme of compression spring [24].

The force $F_s$ produced by a linear elastic spring along its length $x$ with a constant $K_s$ (see Fig. 4.11.)

$$F_s = K_s x \tag{4.69}$$

where: $x$ - space available when the spring is compressed
$K_s$ - spring constant or trial rate, which is a measure of a spring's stiffness. It can be determined by:

$$K_s = \frac{Gd^4}{8ND^3} \tag{4.70}$$

where: $G$ - modulus of elasticity (according to the material and wire diameter)
$d$ - wire diameter
$D$ - mean coil diameter
$N$ - number of active coils determined by the type of ends on a compression spring. If the ends are to be closed and ground

$$N = TC - 2 \tag{4.71}$$

$TC$ - total coils that the spring can contain, which is the ratio between the length of the spring and the diameter of the wire

$$TC = \frac{x}{d} \tag{4.72}$$

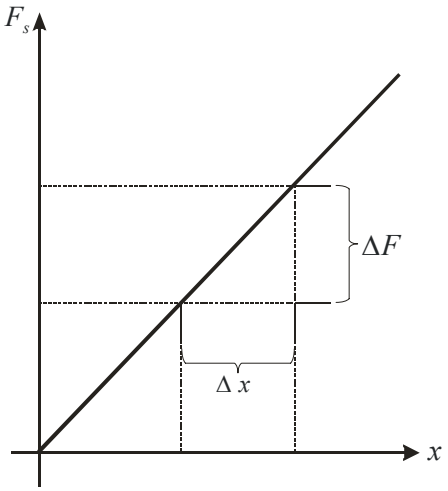


Fig. 4.11. Relation between the displacement and the force acting on a spring.

In the case that the spring works within a tube or cylinder, the spring outside diameter $D_o$ must be less in diameter to keep the spring from jamming in the bore when it is compressed.

The trial mean diameter $D$ is equal to the outer diameter minus the wire diameter

$$D = D_o - d \tag{4.73}$$

The spring index

$$C = \frac{D}{d} \tag{4.74}$$

and $C$ must be kept in the range between 4 and 16. When the spring index is too low, stress problems occur, and when the index is too high, entanglement and waste of material occur.

The working stress $S$ is calculated using the appropriate equation with the working load $F$ applied to the spring

$$S = \frac{8 K_a DF}{\pi d^3} \tag{4.75}$$

where the Wahl stress correction factor applied for round wire is

$$K_a = \frac{4C - 1}{4C - 4} + \frac{0.615}{C} \tag{4.76}$$

If the working stress of the spring is below the maximum allowable stress, the spring is properly designed in relation to its stress level duration operation.

The potential energy $E$ that can be stored in a deflected compression spring is given by the constant spring and by the distance that the spring is compressed

$$E = \frac{K_s x^2}{2} \tag{4.77}$$

Table 4.3. Common Spring Materials and Properties [26]

| Material | Tensile Strength min. $[psi \times 10^3]$ | Modulus of Elasticity $[psi \times 10^6]$ | Modulus in Torsion $[psi \times 10^6]$ | Max. Design Temp. [deg $F$] |
|---|---|---|---|---|
| Music Wire | 229 – 300 | 30 | 11.5 | 250 |
| Chrome Vanadium | 190 – 300 | 30 | 11.5 | 425 |
| Stainless Steel 302 | 125 – 320 | 28 | 10 | 550 |
| Stainless Steel 17-7 (313) | 235 – 335 | 29.5 | 11 | 600 |

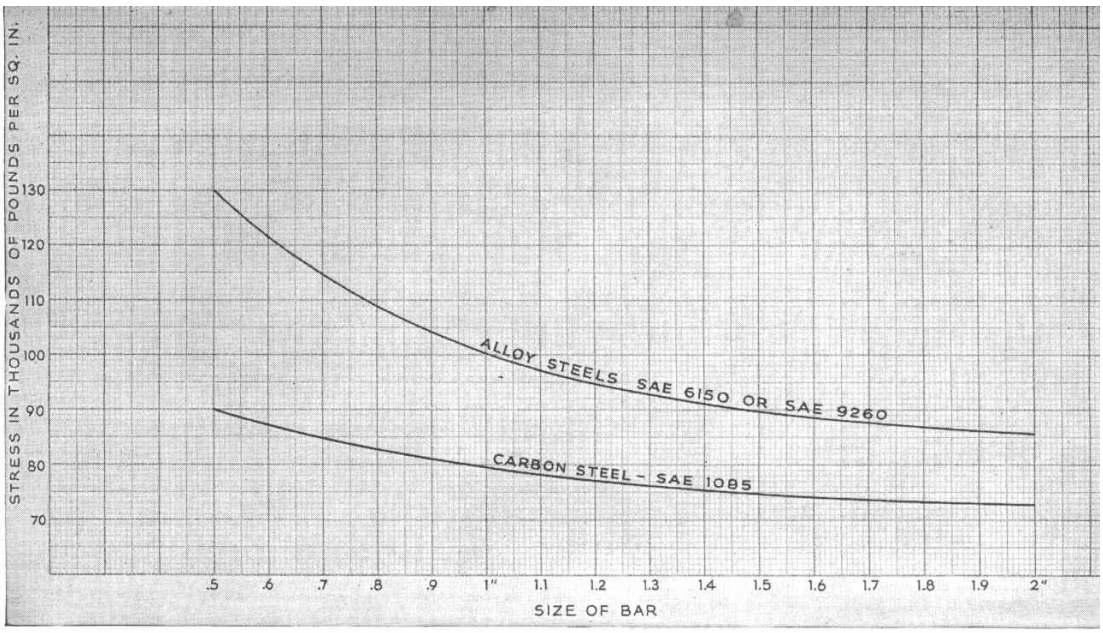


Fig. 4.12. Parameters of compression springs made from hot-rolled bars (maximum allowable stress when solid, Wahl correction not included) [24]

## 4.4 Numerical Calculations of Linear Generator

On the basis of the equations derived in the sections 4.2 and 4.3, computer program (calculations.m) was written using MATLAB in the form of m-file. The program listing is shown in Appendix B. The calculations were done for the long secondary LSG with the reference to the parameters of the currently used mechanical shock absorbers (Chapter 2).

The initial assumed parameters:

- output terminal voltage $V_{out} = 24\ V$
- damping electromagnetic force $F = 1450\ N$
- mutual primary to secondary speed $v = 0.5\ m/s$
- secondary part:
  - permanent magnets made of $Nd - Fe - B$ produced by the German Company Vacuumschmelze type: VACODYM 383 with demagnetized characteristic shown in Fig. 4.3. Data of the magnets:
    - remanent magnetic flux density $B_r = 1.2\ T$
    - coercive force $H_c = 900\ kA/m$
    - temperature $T = 20°\ C$
  - secondary core made of solid iron with infinitive permeability $\mu = \infty$
  - permissible flux density $B_{y2} = 1.2\ T$
  - secondary diameter $D_2 = 48\ mm$
- airgap:
  - airgap flux density $B_g = 0.85\ T$
  - airgap length $g = 1\ mm$
- primary part:
  - phase winding (Fig. 4.13.) with the following data:
    - number of pair poles $p = 4$
    - pole pitch $\tau = 35\ mm$
    - number of slots per pole per phase $q = 1$
    - rated current density $J_{cu} = 6\ A/mm^2$
    - work temperature $T_a = 347°K\ (75°\ C)$
  - primary core made of lamination with negligible power losses and permissible flux density in the yoke $B_{y1} = 1.8\ T$, and in the teeth $B_t = 2\ T$

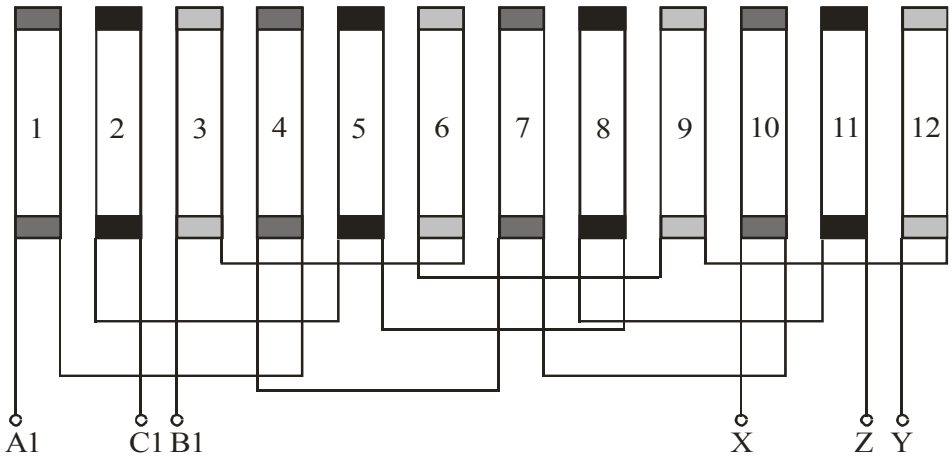


Fig. 4.13. Three-phase core LSM primary winding.

With $K_m = 0.7$ as a proportion of the pole pitch, the magnet width $W_m = 24.5\ mm$ (Eqn. 4.15). For the magnetic flux density in the airgap $B_g = 0.85\ T$, the field intensity $H_m = 262.5\ kA/m$ (Fig. 4.3). According to Eqn. 4.9, the thickness of the permanent magnets $l_m = 4\ mm$. The diameter of the secondary core $D_{y2} = 40\ mm$ (Eqn. 4.28).

The crossection area of the surface for half of the magnetic flux in airgap $A_g = 1767.1\ mm^2$ (Eqn. 4.18). According to Eqn. 4.17 the magnetic flux $\phi = 15\ mW$. If the permissible flux density in primary tooth $B_t = 2\ T$, the crossection area in the primary tooth $A_t = 523.39\ mm^2$ (Eqn. 4.17). Considering the iron coefficient $K_{Fe} = 0.9$, the tooth width $b_t = 3.9\ mm$ (Eqn. 4.20). The tooth pitch $\tau_t = 11.7\ mm$ (Eqn. 4.16), and the slot opening $b_s = 7.8\ mm$ (Eqn. 4.21). The Carter's coefficient $K_c = 1.69$ (Eqn. 4.23), so the equivalent airgap $g_{eq} = 1.7\ mm$ (Eqn. 4.22).

The crossection area of the surface for the magnetic flux in the secondary yoke $A_{y2} = 1300\ mm^2$ (Eqn. 4.27), and the crossection area of the winding surface for half of the magnetic flux $A_{w1} = 200\ mm^2$ (Eqn. 4.31). From Eqn. 4.26, the magnetic flux density in secondary yoke $B_{y2} = 1.25\ T$, and the magnetic flux density on the winding surface $B_{w1} = 0.8\ T$ (Eqn. 4.30).

Taking the emf coefficient as $K_e = 2.5$, the maximum electromotive force of one phase $E_\phi = 35.9\ V$ (Eqn. 4.40). The length of the coil turns on the smooth surface of the equivalent stator core $l_t = 161.4\ mm$ (Eqn. 4.35). For the previous values, the accepted number of turns in a coil $N_c = 70$ (Eqn. 4.34). According to Eqn. 4.33, the constant $K_E = 72\ \ V.s/m$, and the corrected maximum electromotive force per phases $E_\phi = 35.9\ V$ (Eqn. 4.32). The average value of the line electromotive force $E = 59.3\ V$ (Eqn. 4.37).

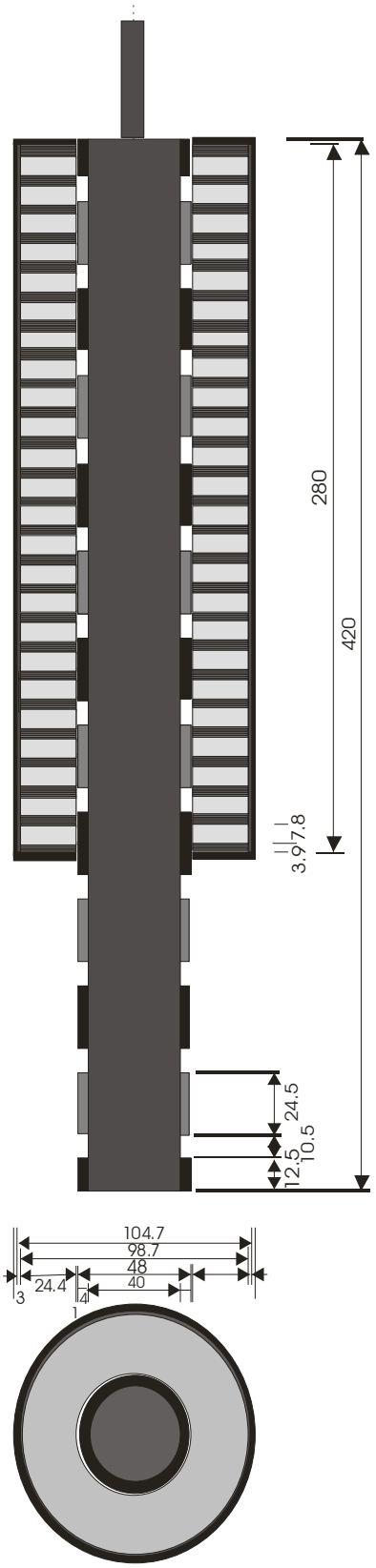


Fig. 4.14. Design data of the permanent magnet linear synchronous generator.

From Eqn. 4.42, the average value of the output current $I = 12\ A$. The rms value of the phase current $I_\phi = 10\ A$ (Eqn. 4.41). The crossection area of the wire $A_w = 1.77\ mm^2$ (Eqn. 4.44), so the wire diameter $D_w = 1.5\ mm$ (Eqn. 4.45). The crossection area of the coil copper $A_{ccu} = 123.7\ mm^2$ (Eqn. 4.46). With a copper coefficient $K_{cu} = 0.65$, the crossection area of the coil $A_c = 190.31\ mm^2$ (Eqn. 4.47). From Eqn. 4.48, the length of the tooth $h_t = 24.4\ mm$. The average coil diameter $D_c = 75.7\ mm$ (Eqn. 4.52). The average length of the coil $l_c = 238\ mm$ (Eqn. 4.51). The length of the wire per phase $l_\phi = 133.26\ m$ (Eqn. 4.50). According to Eqn. 4.58, the primary yoke diameter $D_{y1} = 98.7\ mm$. The thickness of the primary yoke $W_{y1} = 3\ mm$ (Eqn. 4.59), and the outer diameter of the primary $D_{out1} = 104.7\ mm$ (Eqn. 4.60).

From Eqn. 4.49, for a copper conductivity $\sigma = 57x10^6\ Sm$, the phase resistance $R_\phi = 1.3\,\Omega$. The phase resistance adjusted to the operating temperature $R_{\phi T} = 1.6\,\Omega$ (Eqn. 4.53). The per phase inductance $L_a = 6.1\ mH$ (Eqn. 4.54).

The voltage drop across the phase resistance $\Delta V_R = 16\ V$ (Eqn. 4.65), the power losses in the winding $\Delta P_C = 395\ W$ (Eqn. 4.66), and the output power $P_{out} = 330\ W$ (Eqn. 4.67). The generator efficiency $\eta = 46\ \%$ (Eqn. 4.68).

The total length of the primary $l_{prim} = 280\ mm$ (Fig 4.14), and the total length of the secondary $l_{\sec} = 420\ mm$ (Eqn. 4.63). The maximum displacement of the secondary with respect to the primary (the space available when the spring is compressed) $\Delta x = l_{\sec} - l_{prim} = 0.140\ m = 5.5\ in$.

The parameters calculated above are listed in the tables 4.4. and 4.5.

Table 4.4. Main parameters of the generator.

| | |
|---|---|
| Output voltage, $V_{out}$ | $24\ V$ |
| Maximum damping force developed by the generator at speed $0.5\ m/s$, $F$ | $1450\ N$ |
| Maximum secondary speed, $v$ | $0.5\ m/s$ |
| Number of pair poles, $p$ | 4 |
| Voltage and force constant, $K_E$ | $72\ V.s/m$ |
| Phase resistance, $R_\phi$ | $1.3\,\Omega$ |
| Phase inductance, $L_a$ | $6.1\ mH$ |

Table 4.5. Basic dimensions of the generator.

| | |
|---|---|
| Secondary diameter, $D_2$ | 0.048 *m* |
| Diameter of the secondary core, $D_{y2}$ | 0.040 *m* |
| Thickness of the permanent magnets, $l_m$ | 0.004 *m* |
| Airgap, $g$ | 0.001 *m* |
| Length of the tooth, $h_t$ | 0.0244 *m* |
| Thickness of the primary yoke, $W_{y1}$ | 0.003 *m* |
| Diameter of the primary yoke, $D_{y1}$ | 0.0987 *m* |
| The outer diameter of the primary, $D_{out}$ | 0.1047 *m* |
| Pole pitch, $\tau$ | 0.035 *m* |
| Tooth width, $b_t$ | 0.0039 *m* |
| Slot opening, $b_s$ | 0.0078 *m* |
| Vertical length of primary, $l_{prim}$ | 0.280 *m* |
| Vertical length of secondary, $l_{\text{sec}}$ | 0.420 *m* |

## 4.5 Numerical Calculations of Spring

Considering the force produced by the spring $F_s = 1450\ N = 6.3\times10^3\ lb/in$ at maximum displacement, the spring constant $K_s = 10.3\times10^3\ N/m = 1.2\times10^3\ lb/in$ (Eqn. 4.69). The maximum Chrome Vanadium wire diameter $d = 0.5\ in$, so the numbers of coils that the spring can contain $TC = 11\ coils$ (Eqn. 4.72). To keep from jamming the spring, selected are 10 coils, and if the ends are to be closed and ground, the number of active coils $N = 8\ coils$ (Eqn. 4.71). The bore is $4.12\ in$ in diameter, so the spring outside diameter should be smaller to keep the spring from jamming in the bore when it is compressed, and it is $D_o = 4\ in$. If the diameter wire is $0.5\ in$, the trial mean diameter $D = D_o - d = 3.5\ in$ (Eqn. 4.73). This produces a spring index of $C = 7$ (Eqn. 4.74), which is close to the dial index, which must be between $4$ and $16$. Having the spring constant $K_s$, the modulus of torsion $G = 11.5\times10^6\ \ psi$ for Chrome Vanadium, the wire diameter $d$, and the mean coil diameter $D$, from Eqn. 4.70, the number of active coils $N = 2\ coils$. The Wahl stress correction factor applied $K_a = 1.2$ (Eqn. 4.76). The stress $S = 546\times10^3\ \ psi$ (Eqn. 4.75). Since the maximum stress allowable for the diameter Chrome Vanadium $S_{\max} = 190x10^3\ \ psi$ (from Table 4.2), which is smaller than the calculated, it is necessary to made another calculation. One solution is to place another spring inside of the existing spring; the two springs will be in parallel, with their rate (constant spring) added to produce the total rate. The second spring must be in wound-opposite-hand to the existing spring, so that the coils do not tangle or jam. The added spring is calculated in the same way to produce the maximum rate. Another solution is to use hot-wound compression springs. The same formulas for load, stress, and deflection apply to hot-wound springs.

The new calculation is for a hot-wound spring. Taking a bar diameter for Alloy Steel SAE 6150 Chrome Vanadium of $d = 0.9\ in$, the maximum numbers of coils that the spring can contain $TC = 6\ coils$ (Eqn. 4.72). If the ends are to be closed and ground, the number of active coils $N = 4\ coils$ (Eqn. 4.71). The bore is $4.12\ in$ in diameter, and the outside diameter $D_o = 4.12\ in$. If we try $0.9\ in$ diameter bar, the trial mean diameter $D = D_o - d = 3.22\ in = 0.08\ m$ (Eqn. 4.73). This produces a spring index of $C = 3.6$ (Eqn. 4.74), which is close to the dial index, which must be between $4$ and $16$. Having the spring constant $K_s$, the modulus in torsion $G = 10.5 \times 10^6\ psi$, which is less for bars, the wire diameter $d$, and the mean coil diameter $D$, from Equation 4.70 the number of active coils $N = 22\ coils$. The Wahl stress correction factor applied $K_a = 1.46$ (Eqn. 4.76). The stress $S = 106 \times 10^3\ psi$ (Eqn. 4.75), since the maximum stress allowable for diameter of $d = 0.9\ in$ Alloy Steel SAE 6150 Chrome Vanadium $S_{\max} = 104 \times 10^3\ psi$ (from Fig. 4.12), which is the approximate calculation. The available potential energy that can be stored in the spring $E = 18 \times 10^3\ in.lb = 102\ N.m$ (Eqn. 4.77).

The parameters calculated above are listed in the table 4.6.

Table 4.6. Spring parameters.

| | |
|---|---|
| Spring length, $x$ | $0.14\ m$ |
| Spring constant, $K_s$ | $10.3 \times 10^3\ N/m$ |
| Spring trial mean diameter, $D$ | $0.08\ m$ |
| Spring bar diameter, $d$ | $0.9\ in$ |
| Maximum number of coils, $TC$ | $6\ coils$ |

# CHAPTER 5
# ANALYSIS OF OPERATION OF ELECTRIC SHOCK ABSORBER

## 5.1 Performance at Steady-state Conditions

The performance of the designed electric shock absorber should be compare with the mechanical one, and the damping force-speed characteristics (see Fig. 2.5) should be considered. To draw this type of characteristic for the electric shock absorber, the operation of the linear generator at constant speed should be analyzed. Thus, no spring is taken into account.

### 5.1.1 Model of Electric Shock Absorber at Steady-state Conditions

Due to the negligible role of the armature inductance, the generator model at steady state stable conditions can be regarded as the DC generator operating on the DC voltage source with the internal resistance $R_S$ (see Fig. 5.1)

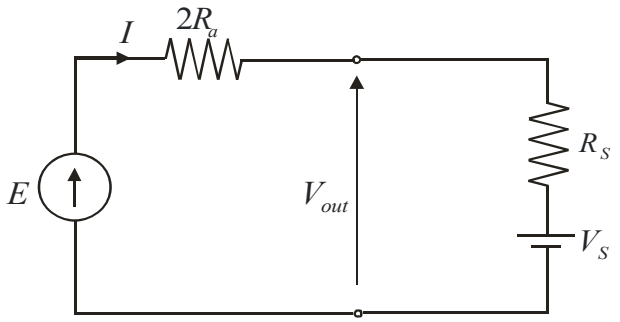


Fig. 5.1. Simplified equivalent circuit of the electric shock absorber without inductances.

In practice, the controlled rectifier connected between the generator and the source will allow adjustment to the voltage at the output terminals of the generator. The source is a battery with an internal resistance $R_s$ and a voltage $V_s$.

The voltage equation for this circuit

$$E = V_S + (2R_a + R_S)I \tag{5.1}$$

Since the emf

$$E = Kv \tag{5.2}$$

and the damping force

$$F_{em} = KI \tag{5.3}$$

the force expressed in terms of the speed, the resistances, and the voltage source has the form

$$F_{em} = K\left(\frac{Kv - V_S}{2R_a - R_S}\right) \tag{5.4}$$

### 5.1.2 Steady State Characteristics of Electric Shock Absorber

For the purpose of this project, the calculations of the force-speed characteristics are made for three different values of the source voltage ($V_S = 0, 12, 24\ V$). For each characteristic, the speed changes from 0 to 1.5 m/s, ($v = 0 - 1.5\ m/s$). The battery resistance is set at $R_S = 0\ \Omega$. The armature resistance $R_a = 1.3\ \Omega$. The constant value is referred to the generator constant as $K = \left(3\sqrt{3}/\pi\right)K_E = 119\ V.s/m$ where $K_E = 72\ \ V.s/m$ is the voltage and force constant (from section 4.4).

On the basis of Eqn. 5.4, a computer program (steady.m) was written using MATLAB in the form of m-file. The program listing is shown in Appendix C. The force-speed characteristics of the electric shock absorber obtained for the parameters indicated are shown in Fig. 5.2.

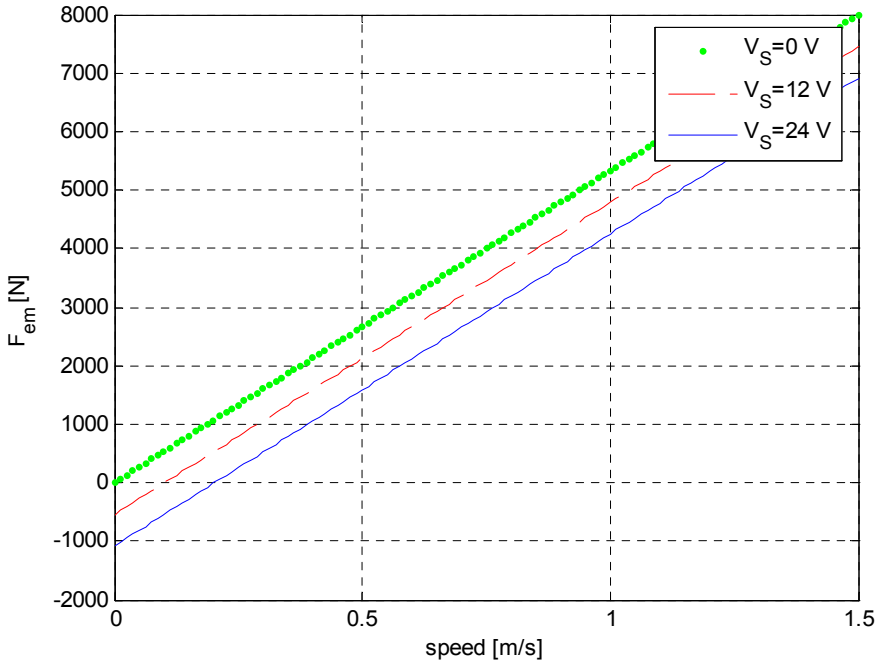


Fig.5.2 Damping force-speed characteristics

Referring to the characteristics of the mechanical shock absorber in Fig. 2.5., the type of curve of the damping force-speed characteristics is a linear one. In general, due to the controlled rectifier, the force-speed characteristic may be modified and adjusted to the particular need. The biggest force appears with the smallest voltage source ($V_S = 0\ V$). If the voltage increases, the force decreases proportionally. The electromagnetic (damping) force calculated at rated conditions: voltage $V_S = 24\ V$

and speed $v = 0.5\ m/s$ is equal to $F_{em} = 1450\ N$, the value assumed in the design calculations in section 4.4.

An important parameter is the quantity of mechanical energy converted to the electrical energy and stored in the battery. This can be partially assessed by calculating the efficiency at the entire electric shock absorber system in the following way:

$$\eta = \frac{P_{out}}{P_{in}} \tag{5.5}$$

where: $P_{out}$ - output power

$$P_{out} = V_S I \tag{5.6}$$

$P_{in}$ - input power

$$P_{in} = F_{em} v \tag{5.7}$$

On the basis of Eqns. 5.5, 5.6 and 5.7, the steady.m computer program plots the efficiency-speed characteristic for two different values of the source voltage ($V_S = 12\ and\ \ 24\ V$). The efficiency-speed characteristics of the electric shock absorber obtained for the parameters indicated are shown in Fig. 5.3.

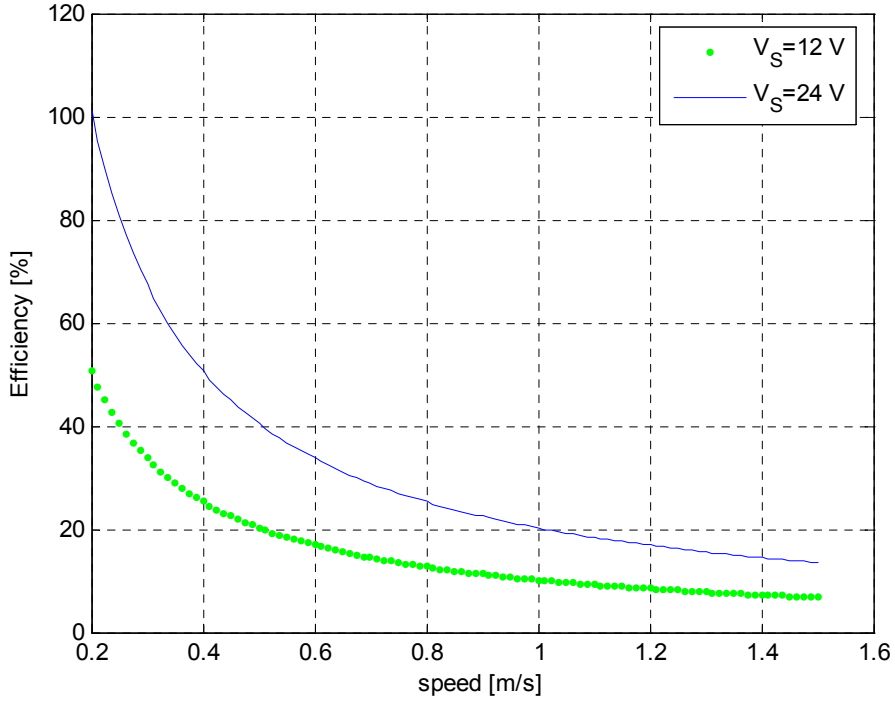


Fig.5.3 Efficiency-speed characteristics

The type of curve of the efficiency-speed characteristics is exponential, and the efficiency decreases inversely proportional to the speed. The greatest efficiency appears with the smallest speed. The transfer of energy from the generator to the battery occurs when $E > V_S$. Since $E = Kv$, and $K = 119\,V.s/m$, the generator starts to send the energy to the battery at speed $v = 0.2\,m/s$. This explains why the efficiency-speed characteristic is drawn for speed $v \geq 0.2\,m/s$. It must be pointed out that the motion losses (friction losses) were not considered in the calculation. This explains why at speed $v = 0.2\,m/s$ with voltage source $V_S = 24\,V$, the efficiency tends to $\eta = 100\,\%$. Certainly, in practice, the efficiency is close to zero, since no power transfer occurs, and only mechanical losses exist. The efficiency calculated at rated conditions: voltage $V_S = 24\,V$ and speed $v = 0.5\,m/s$ is equal to $\eta = 40\,\%$. Therefore, at this speed only $40\,\%$ of the mechanical energy is converted into electrical energy and stored in the battery.

## 5.2 Performance at Dynamic Conditions

The dynamic model of the electric shock absorber should include the spring. Since the road conditions may change, they will influence the operation of the generator. The variation of the speed will influence the emf $e$, which in turn will affect the current $i$. Due to this, the circuit model of the electric shock absorber should include the inductances. Thus, the equivalent circuit takes the form shown in Fig. 5.4.

### 5.2.1 Mathematical Model

The voltage equation of the circuit of Fig. 5.4.

$$e = V_S + (2R_a + R_S)i + L\frac{di}{dt} \tag{5.8}$$

where $R_S$ and $V_S$ are the resistance and the voltage of source respectively.

The total inductance

$$L = 2L_a \tag{5.9}$$

where $L_a$ - phase inductance, which is approximately equal to the leakage inductance expressed by equation 4.54.

The emf $e$ is composed of maximum values of the line-to-line voltages that are changing in time as shown in Fig. 4.8. The line-to-line voltages

$$\begin{aligned} e_{AB} &= K_E(\sin(\omega t) - \sin(\omega t - 120°)) \\ e_{BC} &= K_E(\sin(\omega t - 120°) - \sin(\omega t - 240°)) \\ e_{CA} &= K_E(\sin(\omega t - 240°) - \sin(\omega t)) \end{aligned} \tag{5.10}$$

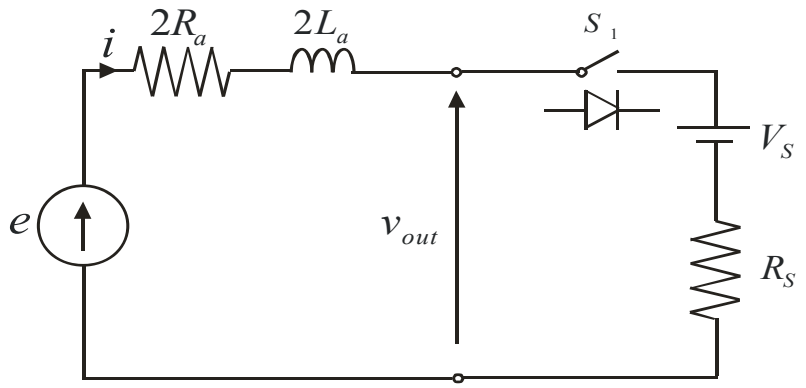


Fig. 5.4. Simplified equivalent circuit of electric shock absorber with switch $S_1$ working as a diode.

So that the current does not flow in the opposite direction, when the machine begins to work as a motor, the Switch $S_1$ is added to the circuit 5.4. This switch works as a diode. The switch is closed and lets the current flow only when the electromotive force $e$ is bigger than the voltage source $V_S$ (if $e > V_S \Rightarrow S_1\ ON$).

The mechanical system is shown schematically in Fig 5.5.

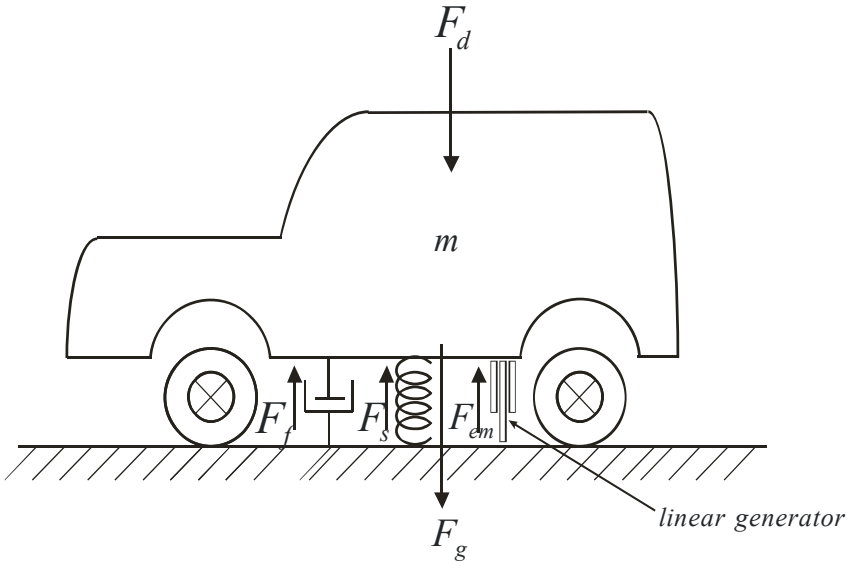


Fig. 5.5. Mechanical model of the electric shock absorber

The force equation of this system is as follows:

$$F_g + F_d = F_{em} + m\frac{d^2x}{dt^2} + F_f + F_S \tag{5.11}$$

where: $m$ - mass of the body

$F_{em}$ - electromagnetic force

$$F_{em} = K_E i \tag{5.12}$$

$K_E$ - voltage and force constant

$i$ - output current

$F_g$ - gravity force

$$F_g = mg \tag{5.13}$$

$g$ - gravity constant

$F_d$ - driving force

$F_s$ - spring force

$$F_s = K_s x \tag{5.14}$$

$K_s$ - spring constant

$x$ - displacement of the secondary with respect to the primary of the PMLSG

$F_f$ - friction force

$$F_f = vD \tag{5.15}$$

$D$ - friction constant

$v$ - relative speed of the primary and the secondary parts of the PMLSG

The instantaneous input power

$$p_{in} = ei \tag{5.16}$$

where: $e$ - electromotive force

The instantaneous output power

$$p_{out} = V_{out} i \tag{5.17}$$

where: $V_{out}$ - output voltage

### 5.2.2 Dynamic Characteristics of Electric Shock Absorber

The simulation of the electric shock absorber was carried out in MATLAB using SIMULINK. The block diagram shown in Fig. 5.6 was built with the reference to the equations written for dynamic model.

The multiplexor was used to stack the current $i$, the induced voltage $e$, the input power $P_m$, the linear speed $v$, the displacement $x$, the electromotive force $F_{em}$, the spring force $F_S$, the friction force $F_f$, the driving force $F_D$, and the time $t$, into a vector and to display the plots. A temporary storage in array named $y$ is used in the MATLAB workspace. The plots are generated by the MATLAB commands in the drawings.m file, as shown in Appendix D.

To examine the operation of the electric shock absorber at dynamic conditions the step response to the driving force was studied. The parameters of the entire system were set up as follows:

- armature resistance $R_a = 1.3\ \Omega$.
- armature inductance $L_a = 6.1\ mH$
- voltage and force coefficient $K_E = 72\ V.s/m$
- mass $m = 100\ Kg$
- spring constant $K_S = 10.3 \times 10^3\ N/m$
- friction coefficient $D = 0.12\ N/m$
- gravitational coefficient $g = 9.8\ m/s^2$
- source resistance $R_S = 0\ \Omega$
- source voltage $V_S = 12\ V$

The driving force that represents the dynamic force acting on the shock absorber when the moving car meets the bump on the road was assumed to be $F_D = 1450\ N$, and it occurred $0.5$ sec after simulation had started. The results of simulations are presented in Figs. 5.7, 5.8, 5.9 and 5.10 in the form of waveforms of the following quantities: shock absorber displacement $x$, speed $v$, current $i$, and electromagnetic force $F_{em}$.

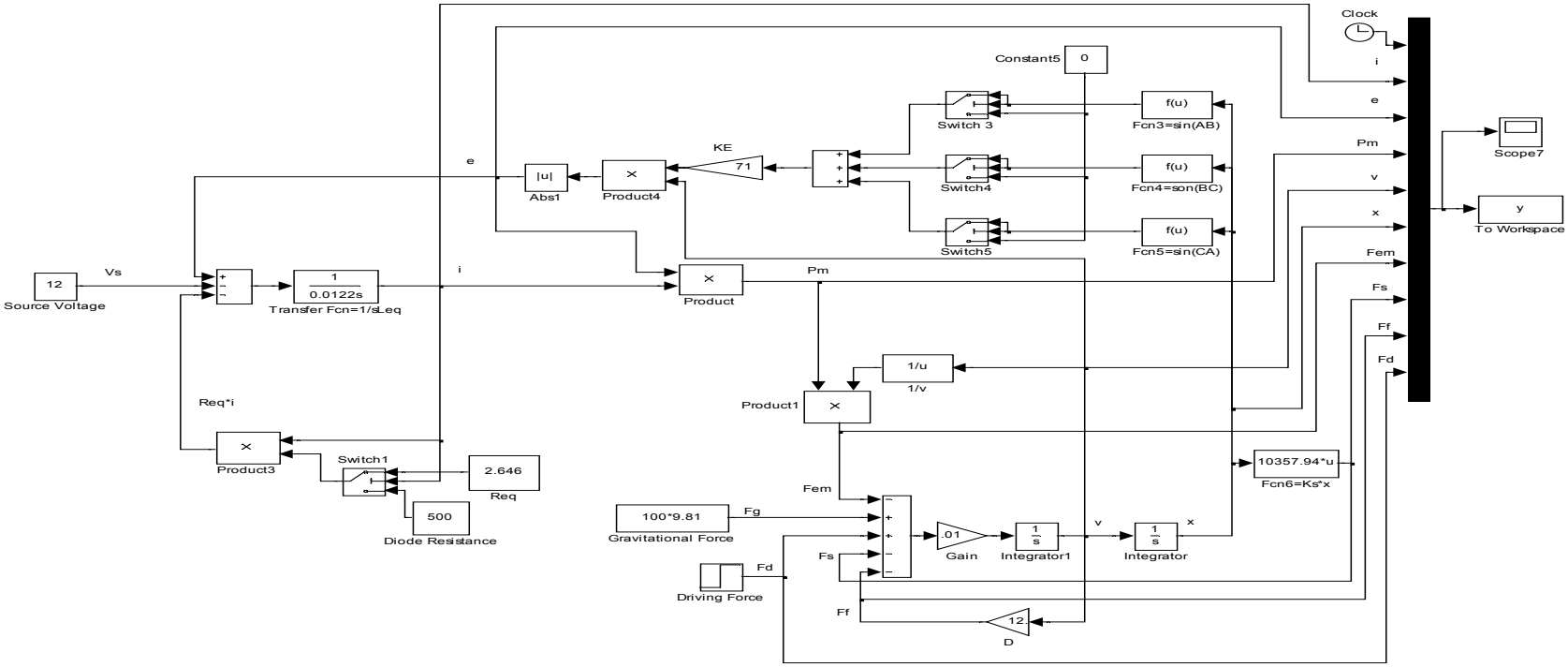


Fig. 5.6. Block diagram of the electric shock absorber in SIMULINK.

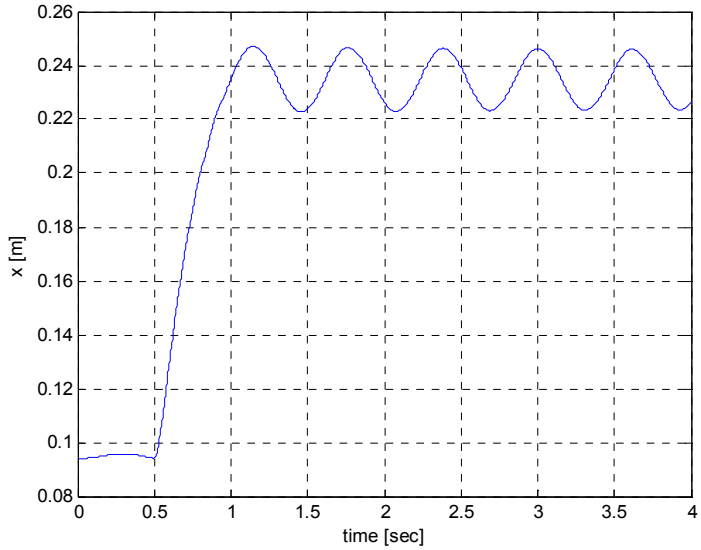


Fig. 5.7. Displacement of the secondary with respect to the primary of the PMLSG

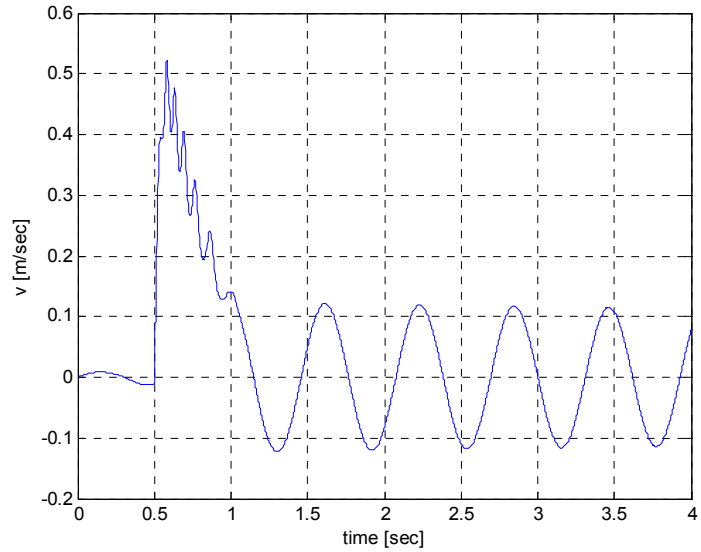


Fig. 5.8. Relative speed of the generator moving parts.

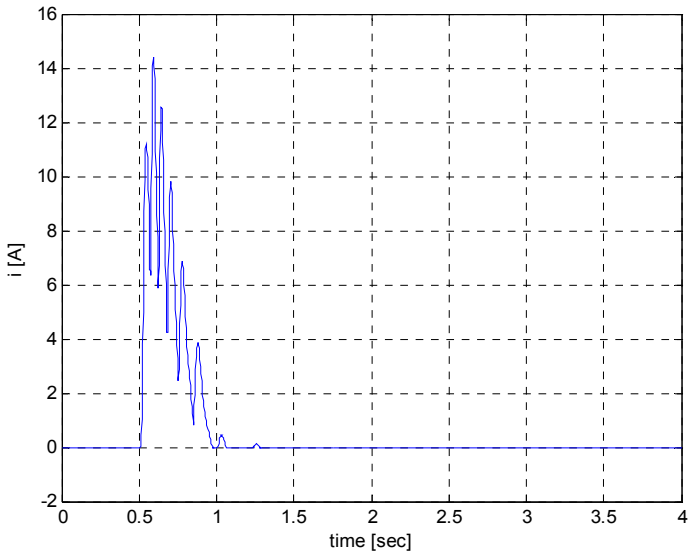


Fig. 5.9. Generator output current

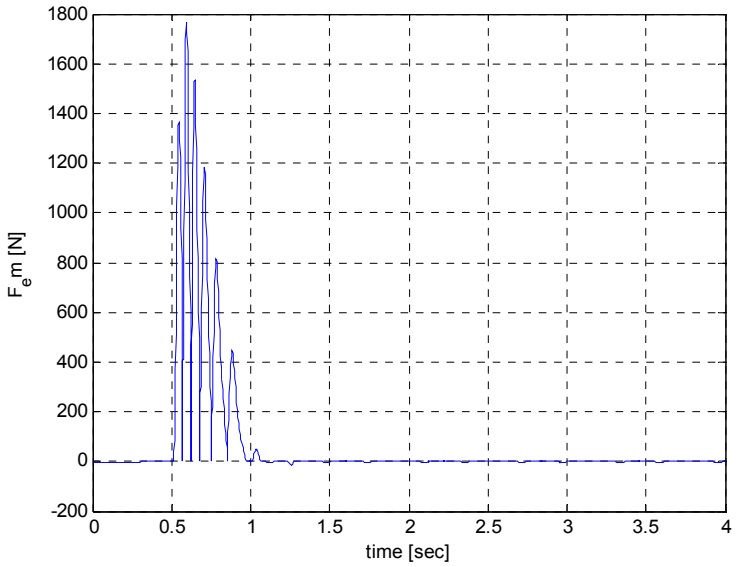


Fig. 5.10. Electromagnetic (damping) force of the generator

The waveform of the displacement $x$ indicates that after disturbance occurred, the oscillations damped until the electromotive force was greater than the source voltage $e > V_S$, these oscillations happen if the speed of the moving part of the linear generator exceeds the certain value of the speed. Below this value, the induced voltage is equal or smaller than the source voltage ($e \leq V_S$); the current drops to 0, and no damping force $F_{em}$ is produced, resulting in steady oscillations of the mechanical system (see Figs. 5.7 and 5.8).

The oscillations are damped to zero if the source voltage $V_S = 0\,V$ (the PMLSG is short-circuited). The results obtained from simulations under this condition are shown in Figs. 5.11, 5.12, 5.13, and 5.14.

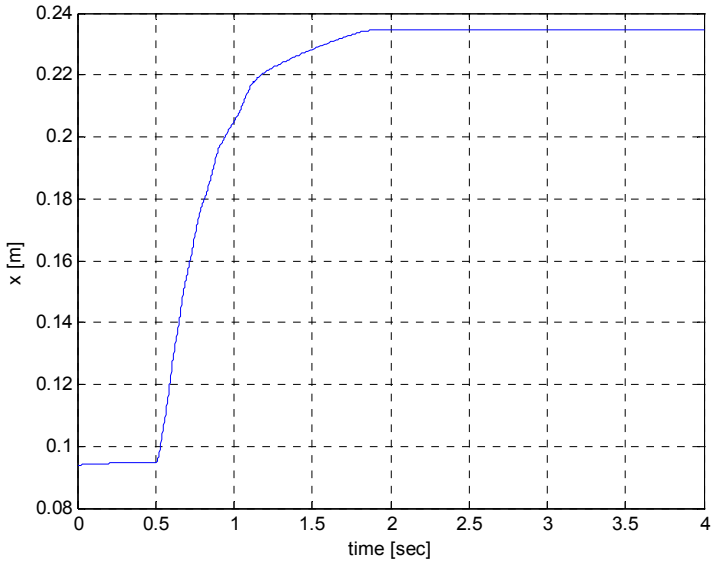


Fig. 5.11. Displacement of the secondary with respect to the primary of the generator with short-circuited winding.

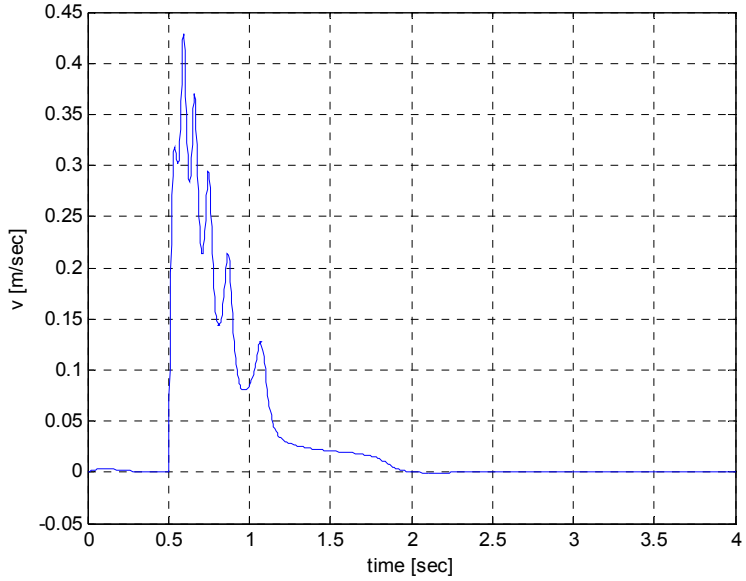


Fig. 5.12. Relative speed of the generator with short-circuited winding.

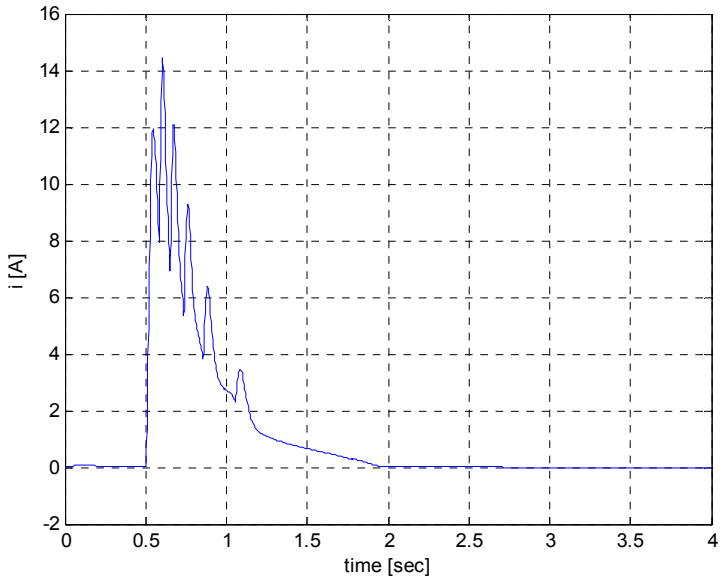


Fig. 5.13. Generator output current with short-circuited winding.

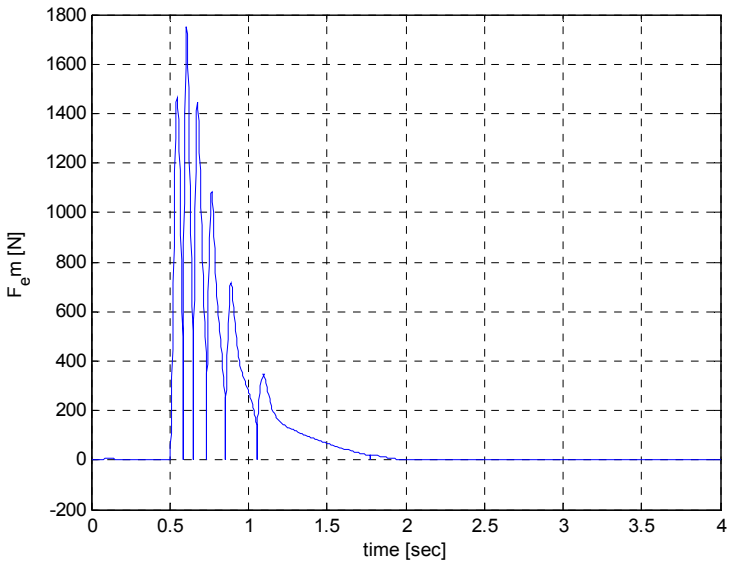


Fig. 5.14. Electromagnetic (damping) force of the generator with short-circuited winding

The electric circuit was modified, in order to ensure the proper conditions of the operations of the electric shock absorber, and to make the shock absorber charges the battery and damp the oscillations.

### 5.2.3 Electric Shock Absorber with Modified Electric Circuit

The modified equivalent circuit of the electric shock absorber is shown in Fig. 5.15. The shunt resistor $R_c = 30\ \Omega$ is connected to the source voltage through the switch $S_2$.

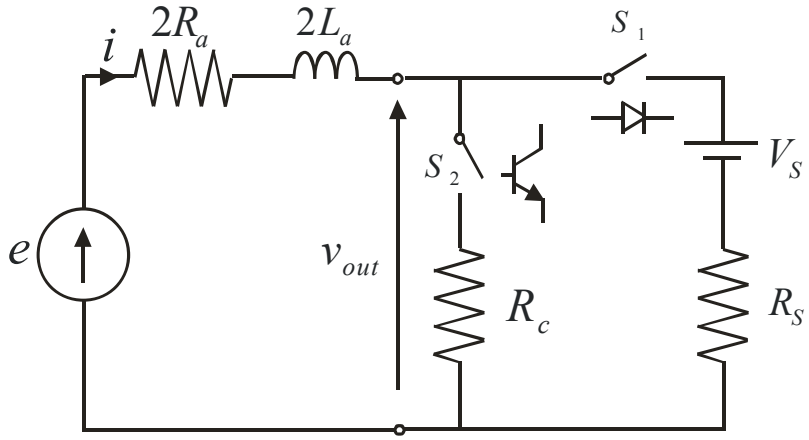


Fig. 5.15. Simplified equivalent circuit of the generator with modified electric circuit (switch $S_2$ works as a transistor).

During the operation

$$if \quad e > V_S \quad \Rightarrow \quad S_1\ ON \quad and \quad S_2\ OFF \tag{5.18}$$

and

$$if \quad e \le V_S \quad \Rightarrow \quad S_1\ OFF \quad and \quad S_2\ ON \tag{5.19}$$

The voltage equation for the operation defined by formula 5.19 is as follows

$$e = (2R_a + R_c)i + L\frac{di}{dt} \tag{5.20}$$

The block diagram of the system with the modified electric circuit is shown in Fig. 5.16. The results obtained from simulation carried out for the modified circuit are shown in Figs. 5.17, 5.18, 5.19, and 5.20. Looking at the displacement waveform shown in Fig. 5.17, it is possible to see that the oscillations that occur after the disturbance is introduced are damped to zero after a short time. The modification of the circuit allows the accumulation of part of the electric energy in the battery, but a large amount of the generated electric energy is dissipated in the winding and in the shunt resistance $R_c$.

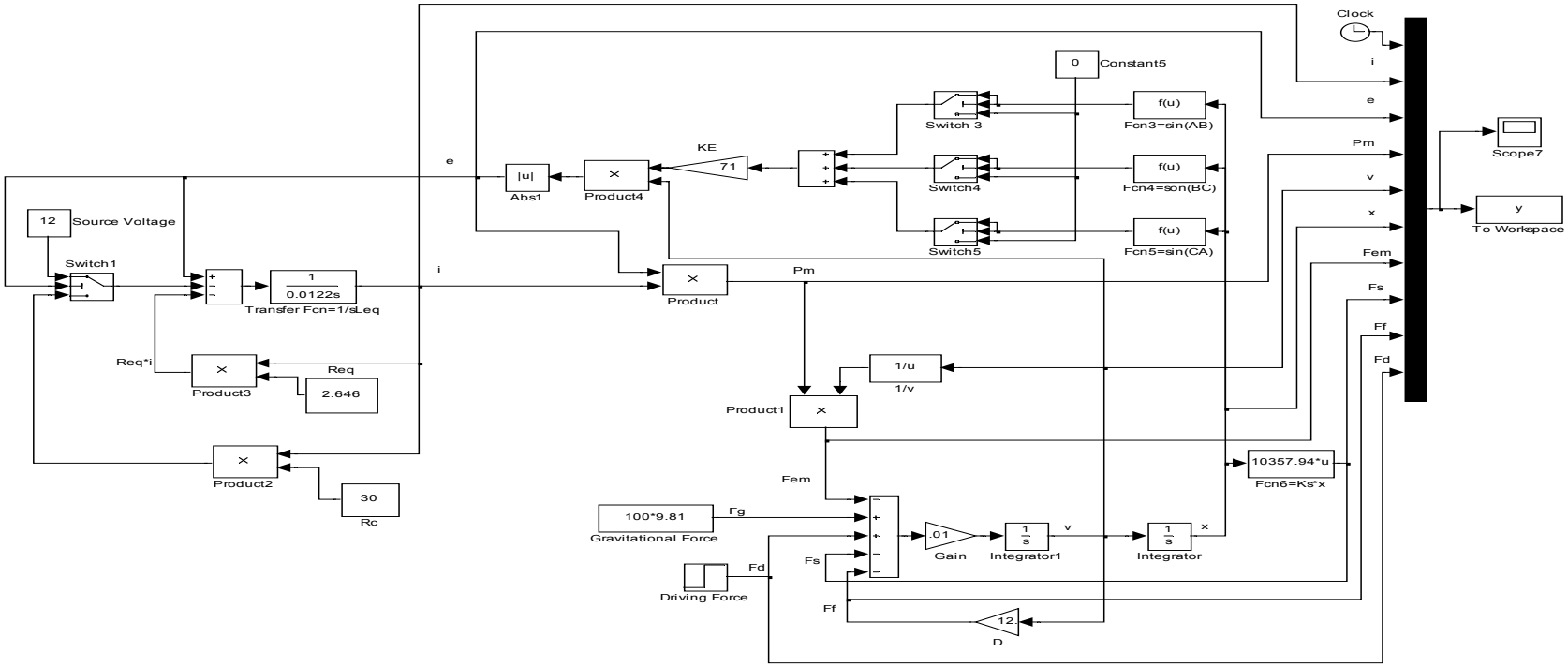


Fig. 5.16. Block diagram of the electric shock absorber in SIMULINK related to Fig. 5.15.

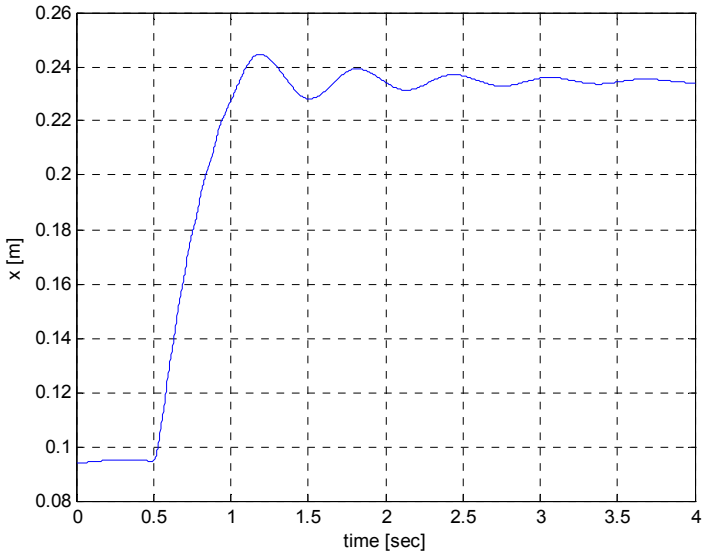


Fig. 5.17. Displacement of the secondary with respect to the primary of the PMLSG with the modified circuit.

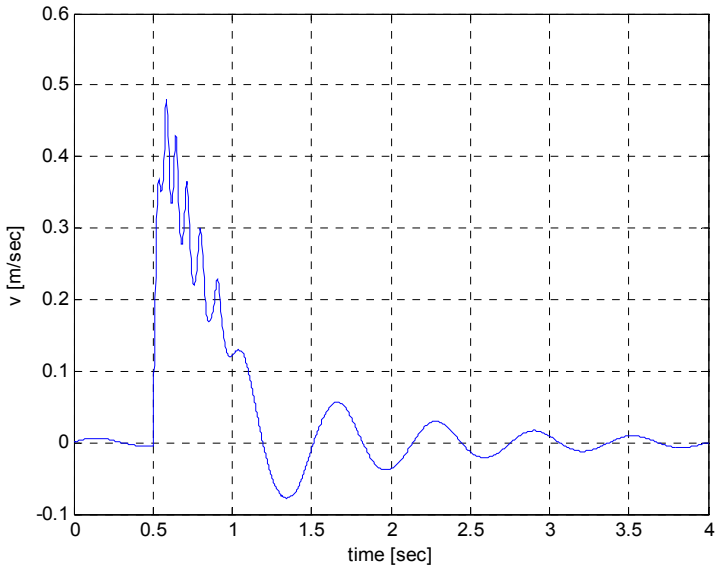


Fig. 5.18. Relative speed of the generator with the modified circuit.

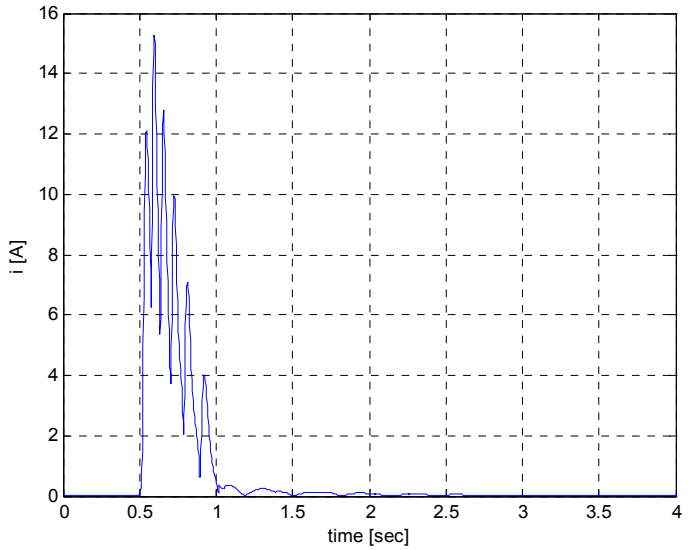


Fig. 5.19. Generator output current with the modified circuit.

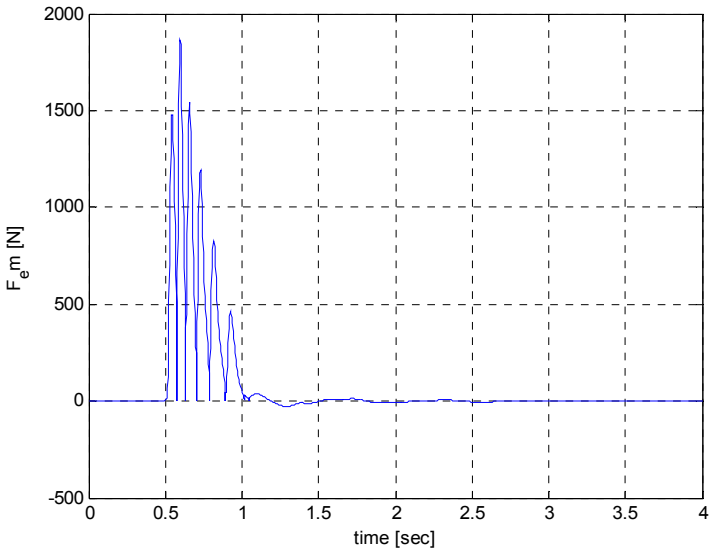


Fig. 5.20. Electromagnetic (damping) force of the generator with the modified circuit.

# CHAPTER 6
# CONCLUSION

An electric shock absorber has been designed and analyzed to use in electric cars. It consists of a permanent magnet linear synchronous generator, a spring, and an electric accumulator. The electric accumulator consists of a controlled rectifier and a battery, and it was not evaluated in the present project. In the design calculations, the dimensions and performance parameters of the currently used mechanical shock absorbers were used as the reference. For this purpose, these shock absorbers were described first.

Five different structures of PMLSGs were studied qualitatively, and the version that best suits the operation within the shock absorber system was selected. This version was the next subject of the design calculation. It is the permanent magnet 3-phase linear synchronous generator with an internal secondary part, a slotted primary core, and a longer secondary side. The permanent magnets, which were applied, are made of a neodymium-iron-boron ( $Nd-Fe-B$ ), produced by German Company Vacuumschmelze. The generator operates on $24\,V$ battery via controlled 3-phase rectifier. The designed spring that the generator operates was a hot-wound compression spring of Alloy Steel SAE 6150 Chrome Vanadium with closed and ground ends.

The designed electric shock absorber was analyzed under steady-state conditions. This allowed the determination of the performance characteristic (force-speed) that characterizes the conventional shock absorber. The results obtained from calculations indicate that the electric shock absorber has a linear characteristic. With the controller rectifier, the force-speed characteristic can be modified and adjusted to the actual road conditions. The calculation results also show that a rated conditions, around $40\,\%$ of the oscillation energy can be converted into electrical energy that charges the battery. However, this parameter depends on the generator secondary part speed.

The electric shock absorber normally operates under dynamic conditions. This was simulated using MATLAB-SIMULINK program. The simplified block diagram model of the shock absorber was analyzed. During simulations, after step disturbance force was applied to the system, the parameters such as output current, electromagnetic (damping) force, displacement, and speed of the electric shock absorber were studied. The simulation results indicate that if the output terminals of the rectified voltage are connected directly to the battery, then the shock absorber does not operate properly and some oscillations are not damped to zero. To make it work properly, an additional resistor was connected parallel to the battery via controlled switch (transistor). After this modification, if the generated voltage by the generator is greater than the battery voltage, the current flowed through the battery. If the generated voltage was smaller or equal to the battery voltage, the additional switch was closed and the generator current flowed through the additional shunt resistor.

The results obtained from the dynamic simulation of the electric shock absorber with the modified output electric circuit show that the oscillations attenuate to zero after disturbance appears. Therefore, the electric shock absorber works properly under the modified circuit.

This thesis is only a small portion of the growing research in this area. It is hoped that the results obtained here will lead to the realization of a better structure of the generator with higher efficiency, the comprehensive study of the electric accumulator, and the evaluation of the feasibility and cost of the entire electric shock absorber. To asses the energy that can be saved by the electric shock absorber, a random function has to be applied as a driving force and the calculation of the average energy must be done. Although, in this kind of generator the induced voltage is nearly sinusoidal, and the high harmonics can be ignored for different structures, they must be included in the future work.

## REFERENCES


[1] Reimpell, J., Stoll, H., and Betzler, J., "The automotive Chassis, Engineering Principles", Second Edition, 2001, pp. 347-385

[2] Crouse, W. and Anglin, D., "Automotive: Chassis and Body," Fifth Edition, McGraw-Hill Book Company, 1976, pp. 48-54

[3] Mendrela, E. and Drzewoski, R., "Electric Shock Absorber for Electric Vehicles," Conference, Proc. of BASSIN' 2000, Lodz, Poland 2000.

[4] Gieras, J. and Wing, M. "Permanent Magnet Motor Technology, Design and applications," Second Edition, Eastern Hemisphere Distribution, 2002. pp. 51-52

[6] Boldea, I. and Nasar, S., "Linear Electric Actuators and Generators," Cambridge University Press, 1977, pp. 46

[7] Mendrela, E., Handouts on Leakage Inductance of the generator winding.

[9] Danielson, O., "Design of a Linear Generator for Wave Energy Plant," Master Degree Project, Uppsala University School of Engineering, UPTEC F03 003, January 2003

[10] Engelmann, R. and Middendorf, W., "Handout of Electric Motors," Department of Electrical and Computer Engineering University of Cincinnati, Ohio, 1995, pp. 334-345

[11] Franklin, G., Powel, D., and Emami-Naeini, A., "Feedback Control of Dynamic Systems," Fourth Edition, Prentice Hall Inc., New Jersey, 2002, pp. 24

[12] Gieras, J. and Piech, Z., "Linear Synchronous Motors," CRC Press, 1999. pp. 1-32

[13] Danielson, O., Thorburn, K., Eriksson, M., and Leijon, M., "Permanent magnet fixation concepts for linear generator," Division for Electricity and Lighting Research. Department of Engineering Sciences Uppsala University, Box 534, S-751 21

[14] Ho-Yong, C., Sang-Yong, J., and Hyun-Kyo, J., "Performance Evaluation of Permanent Magnet Linear Generator for Charging the Battery of Mobile Apparatus," Electric Machines and Drives Conference, 2001. IEEE International

[15] Ivanova, I., Agren, O., Bernhoff, H., and Leijon, M., "Simulation of a 100 kW permanent magnet octagonal linear generator for ocean wave conversion," Division of Electricity and Lighting Research Uppsala University, Sweden.

[16] Mendrela, E., Lukaniszyn, M., and Macek-Kaminsta, K, "Dis-Type Brushless DC Motors," Polish Academy of Science, 2002

[17] Nasar, S. A. and Boldea, I., "Linear Motion Electric Machines," Wiley-Interscience Publication, 1976, pp. 134-159

[18] Parker, R., "Advances in Permanent Magnetism," John Wiley & Sons, 1990

[19] Say, M., "Alternating Current Machines," Fifth Edition, John Wiley & Sons, New York, 1983, pp. 575-591

[20] "Archimedes Waveswing - AWS//BV," 2003. Available at: http://www.waveswing.com

[21] Polinder, H., Damen, M., and Gardner, F., "Modeling and test results of the AWS linear PM generator system," accepted for IEEE transactions on Energy Conversion.

[22] Vacuumschmelze – Rare – Earth Permanent Magnets. VACODYM-VACOMAX Catalog

[23] "Shock Absorbers," 2003. Available at: http://www.monroe.com/tech_support/tec_shockabsorbers.asp

[24] "Handbook of Mechanical Spring Design," Associated Spring Corporation, General Offices, Bristol, Connecticut 06012, 1964, pp. 50-51

[25] Walsh, R., "Electromechanical design handbook," Second Edition, McGraw-Hill, Inc., 1995, pp. 7.1-7.45

[26] "Design and Engineers Resources," 2004. Available at: http://www.engineersedge.com/

## APPENDIX A
## LEAKAGE INDUCTANCE OF THE GENERATOR WINDING

The inductance is expressed by the equation

$$L = \frac{\lambda}{i} \tag{A.1}$$

where $i$ is the current, and $\lambda$ is the flux linkage

The numbers of turns $N(x)$ (Fig. A.1) at any distance $x$ is

$$N(x) = \frac{N_c}{h_t} x \tag{A.2}$$

where $N_c$ is the number of turns in the slot, and $h_t$ its height

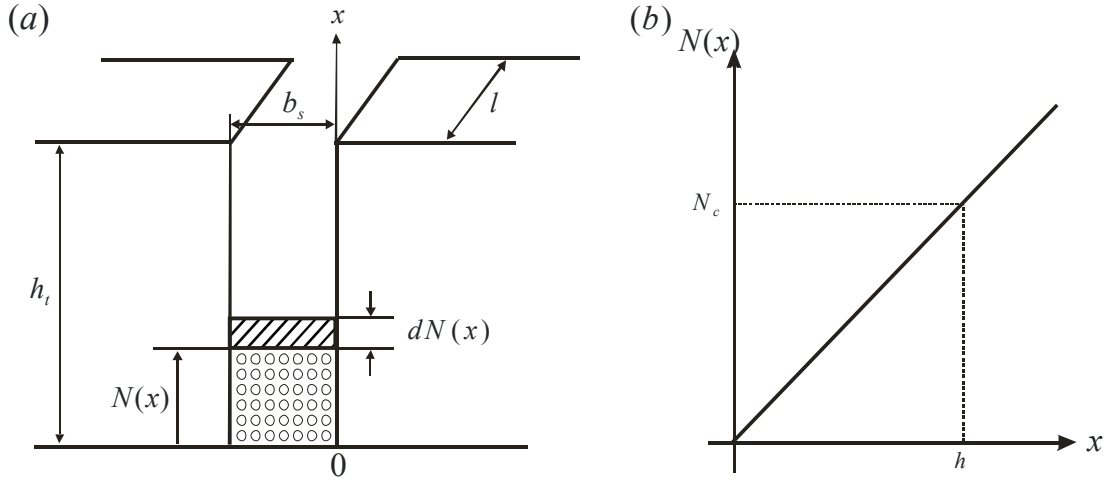


Fig. A.1. (a) Scheme of the slot of the generator primary part, and (b) relation between the number of slots wire and the slot depth

The flux linkage differential at distance $x$

$$d\lambda(x) = N(x)d\phi(x) \tag{A.3}$$

and the flux differential

$$d\phi(x) = d(F(x)\Lambda(x)) \tag{A.4}$$

where: $\Lambda(x)$ - permeance of the leakage flux path

$$\Lambda(x) = \frac{\mu_0 (h_t - x) l}{b_s} \tag{A.5}$$

$b_s$ - width of the rectangular slot
$l$ - length of the slots of the generator

$$l = 2\pi \frac{D_c}{2} q 2p \tag{A.6}$$

$F(x)$ - magnetomotive force

$$F(x) = iN(x) \tag{A.7}$$

After substitution of (A.2) in (A.7),

$$F(x) = i \frac{N_c}{h_t} x \tag{A.8}$$

after differentiating (A.8)

$$dF(x) = i \frac{N_c}{h_t} dx \tag{A.9}$$

Substitution of (A.5), (A.9) into (A.4) gives

$$d\phi(x) = \frac{\mu_0 (h_t - x) l}{b_s} i \frac{N_c}{h_t} dx \tag{A.10}$$

By substitution of (A.2), (A.10) into (A.3)

$$d\lambda(x) = \frac{N_c}{h_t} x \frac{\mu_0 (h_t - x) l}{b_s} i \frac{N_c}{h_t} dx \tag{A.11}$$

The total flux linkage is

$$\lambda = \int_0^{h_t} \lambda(x) dx \tag{A.12}$$

and from (A.11) and (A.12)

$$\lambda = \left( \frac{N_c}{h_t} \right)^2 \frac{\mu_0 l}{b_s} i \int_0^{h_t} (h_t x - x^2) dx \tag{A.13}$$

After integration

$$\lambda = \left( \frac{N_c}{h_t} \right)^2 \frac{\mu_0 l}{b_s} i \left( \frac{h_t x^2}{2} - \frac{x^3}{3} \right) \Bigg|_0^{h_t} \tag{A.14}$$

and finally

$$\lambda = N_c{}^2 \frac{l h_t}{6 b_s} \mu_0 i \tag{A.15}$$

According to (A.1) and (A.15), the leakage inductance is

$$L_l = N_c{}^2 \frac{l h_t}{6 b_s} \mu_0 \tag{A.16}$$

By substitution of (A.6) in (A.16), the leakage inductance takes the form

$$L_l = N_c{}^2 \frac{h_t}{6 b_s} \mu_0 2\pi D_c qp \tag{A.17}$$

## APPENDIX B
## CALCULATIONS.M

```
% Program to design a permanent magnet linear synchronous generator

% Assumed Data

% secondary diameter, air-gap, .....
D2=0.048;              % secondary part outer diameter
g=0.001;               % air-gap
tau=0.035;             % pole pitch
p=4;                   % number of pole pair

% mechanical parameters
v=0.5;                 % secondary speed
F=1450;                % electromagnetic force

% primary winding
m=3;                   % number of phases
q=1;                   % number of slots/pole/phase
Vout=24;               % output voltage
Jcu=6000000;           % current density
Kcu=0.65;              % copper coefficient = coil copper crossection area/ coil
crossection area
Gamcu=57*1000000;      % copper conductivity
T1=272+75;             % work temperature for the winding in Kelvine's degree

% permanent magnets
Bg=0.85;               % flux density in the air-gap
Br=1.2;                % residual flux density
Hc=900*1000;           % coersive force (coercivity)
Wm=0.7*tau;            % magnet width

% flux densities
By1=1.8;               % permissible flux density in primary yoke
By2=1.2;               % permissible density in secondary yoke
Bt=2;                  % permissible density in primary tooth
Kfe=.9;                % iron coefficient = laminated core iron crossection area/
laminated crossection area
mio=4*pi*0.0000001;    % vacum magnetic permeability


%%%%%%%%%%%%%%%%%%%%%%%%%%%%%%%%%%%%%%%%%%%%%%%%%%%%%%%%%%%%%%%%%%%%%%%%%%%%
%%%%%%%%%%%%%%%%%%%%%%%%%%%%%%%%%%%%%%%%%%%%%%%%%%%%%%%%%%%%%%%%%%%%%%%%%%%%
```

```
% Design Calculations

% Magnetic circuit
taut=tau/(q*m);                 % tooth pitch
bt=(1/Kfe)*Wm*Bg/Bt/2;          % tooth width
bs=taut-bt;                     % slot opening
Kc=taut*(5*g+bs)/(taut*(5*g+bs)-bs^2);        % Carter's coefficient
geq=Kc*g;                       % equivalent air-gap
Hm=Hc*(Br-Bg)/Br
lm=(geq*Bg)/(mio*Hm)            % thickness of magnet
lm=input('set lm=')             % corrected thickness of magnet
Dy2=D2-2*lm;                    % diameter of the secondary core
Ag=pi*D2*(Wm/2)                 % cross-section area of the surface for half of
                                magnetic flux in air-gap
At=Bg*Ag/Bt
Ay2=pi*(Dy2/2)^2                % cross-section area of the surface for magnetic flux
                                in secondary yoke
Aw1=pi*(D2+2*geq)*(Wm/2)        % cross-section area of the surface for half of
                                magnetic flux on the winding surface (stator area)
By2=Bg*(Ag/Ay2);                % flux density in secondary core (yoke)
Bw1=Bg*(Ag/Aw1);                % flux density on the winding surface

% Primary winding
% E=Vout+2*(Rp*Irms)=Ke*Vout - emf expressed as an increase of the output
                                voltage
Ke=input('Ke=')                 % emf coefficient, Ke>1
Emp=Ke*(Vout*pi/3)/sqrt(3);     % maximum emf of one phase
lt=pi*(D2+2*geq);               % length of the coil turn (on the smooth surface of
                                the equivalent stator core)
Nc=Emp/(Bw1*lt*2*p*q*v)         % number of turns per coil
Nc=input('set Nc=')
Np=Nc*2*p*q;                    % number of turns per phase
K=Nc*(Bw1*lt*2*p*q);            % generator constant
Emp=K*v;                        % corrected emf
E=sqrt(3)*Emp*(3/pi);           % average value of line emf
I=(pi/3)*F/(sqrt(3)*Bw1*Nc*lt*2*p*q); % average value of the output current
Iprms=sqrt(2/3)*I;              % rms phase current
Aw=Iprms/Jcu                    % crossection area of the wire
Dw=2*sqrt(Aw/pi)                % wire diameter
Dw=input('set Dw=')
Aw=pi*(Dw/2)^2                  % corrected crossection area of the wire
Accu=Nc*Aw                      % crossection area of the coil copper
Ac=Accu/Kcu                     % crossection area of the coil
ht=Ac/bs;                       % length of the tooth
Dc=D2+2*geq+ht;                 % average coil diameter
lc=pi*Dc;                       % average length of the coil
```

```
lp=lc*Nc*2*p*q;                 % length of the wire per phase

%Length of the shock absorber
lpr=taut*(Np/Nc)*m;             % total length of the primary
lsecact=tau*2*p;                % length of active part of the secondary
lsec=tau*2*(p+2);               % length of the secondary

%Equivalent circuit
Rp=lp/Aw/Gamcu;                 % phase resistance at ambient temperature
                                (272+20)=292 K
Rpt=Rp*(T1-38)/(292-38);    % phase resistance at operating temperature T1 K
L=Nc^2*(ht/(6*bs))*mio*4*pi*(Dc/2)*q*p;             % phase inductance
VR=I*Rp;                        % voltage drop across phase resistance
Vout=(E-2*VR);                  % output voltage
DPw=I^2*2*Rp;                   % power losses in the winding
Pout=Vout*I;                    % output power
PEin=E*I;                       % input power calculated fro the electrical quantities
PFin=F*v;                       % input power calculated fro the mechanical quantities
EffE=Pout/PEin;                 % generator efficiency calculated from electric input
                                power
EffF=Pout/PFin;                 % generator efficiency calculated from mechanical input
                                power

% Dimentions of the primary core
Dy1=D2+2*(g+ht);                % primary yoke diameter
Wy1=(Bg/By1)/Kfe*((pi*D2*Wm/2)/(pi*Dy1)) % thickness of the primary yoke
Wy1=input('set Wy1=')
Dout1=Dy1+2*Wy1;                % outer diameter of the primary

%spring constant
x=lsec-lpr;                     %spring distante
Ks=F/x;                         %spring constant

disp('diameter_dimentions')
Dy2_lm_D2_g_ht_Dy1_Wy1_Dout1=[Dy2 lm D2 g ht Dy1 Wy1 Dout1]
disp('primary_dimentions')
taut_ht_bs_bt_lpr=[taut ht bs bt lpr]
disp('secondary_dimentions')
tau_lm_Wm_lsecact_lsec=[tau lm Wm lsecact lsec]
disp('airgap')
g_Kc_geq=[g Kc geq]
disp('lengths')
lc_lp_lt=[lc lp lt]
disp('areas')
Ag_Aw1_Ay2_Aw_Accu_Ac_At=[Ag Aw1 Ay2 Aw Accu Ac At]
disp('flux_densities')
```

```
Bg_Br_By1_By2_Bt_Bw1=[Bg Br By1 By2 Bt Bw1]
disp('winding_parameters')
Nc_Np_Dw_Dc=[Nc Np Dw Dc]
disp('crossection area of the wire')
Aw=[Aw]
disp('electric_parameters')
Vout_I_Rpt_Rp_Pout_PEin_EffE=[Vout I Rpt Rp Pout PEin EffE]
disp('others electric_parameters')
Ke_K_Emp_E_Iprms_VR_DPw=[Ke K Emp E Iprms VR DPw]
disp('leakage inductance')
L=[L]
disp('constant spring')
Ks=[Ks]
disp('mechanical_parameters')
F_v_PFin_EffF=[F v PFin EffF]
```

## APPENDIX C
## STEADY.M

```
% Program to calculate the steady state characteristics of
% the linear generator

clear all;
close all;
Rs=0;                              % source resistance
Ra=1.3;                            % armature resistance
KE=72;                             % voltage and force coefficient
K=(3*sqrt(3)/pi)*KE;
sp=[];
fr=[];
j=1;
for Vs=0:12:24;                    % source voltage
   speed1=[];
   force1=[];
   for v=0:0.0125:1.5;             %  speed
   speed1=[speed1 v];
   Fem=K*(K*v-Vs)/(2*Ra+Rs);       %  electromagnetic force
   force1=[force1 Fem];
   end
   sp(j,:)=[speed1];
   fr(j,:)=[force1];
   j=j+1;
end
plot(sp(1,:),fr(1,:),'g.',sp(2,:),fr(2,:),'r--',sp(3,:),fr(3,:));
grid;
ylabel('F_e_m [N]')
xlabel('speed [m/s]')
legend('V_S=0 V','V_S=12 V','V_S=24 V')
h2=figure;

spe=[];
frc=[];
po=[];
pi=[];
ef=[];
jj=1;
for Vs=12:12:24;                   % source voltage
   speed2=[];
   force2=[];
   voltage=[];
   current=[];
   powerO=[];
```

```
    powerI=[];
    efficiency=[];
    for v=0.2:0.0125:1.5;              %  speed
    speed2=[speed2 v];
    e=K*v;
    voltage=[voltage e];
    i=(e-Vs)/(2*Ra-Rs);                %  current
    current=[current i];
    Fem=K*(K*v-Vs)/(2*Ra+Rs);          %  electromagnetic force
    force2=[force2 Fem];
    Pout=Vs*i;                         %  output power
    powerO=[powerO Pout];
    Pin=Fem*v;                         %  input power
    powerI=[powerI Pin];
    eff=(Pout/Pin)*100;                %  efficiency
    efficiency=[efficiency eff];
    end
    spe(jj,:)=[speed2];
    frc(jj,:)=[force2];
    po(jj,:)=[powerO];
    pi(jj,:)=[powerI];
    ef(jj,:)=[efficiency];
    jj=jj+1;
end
plot(spe(1,:),po(1,:),'r--',spe(2,:),po(2,:));
grid;
h2=figure;
plot(spe(1,:),pi(1,:),'g.',spe(2,:),pi(2,:));
grid;
h2=figure;
plot(spe(1,:),ef(1,:),'g.',spe(2,:),ef(2,:));
grid;
ylabel('Efficiency [%]')
xlabel('speed [m/s]')
legend('V_S=12 V','V_S=24 V')
```

## APPENDIX D
## DRAWINGS.M

```
%M-file for dynamic THESIS
plot(y(:,1),y(:,3))
ylabel('e [V]')
xlabel('time [sec]')
grid
h2=figure;
plot(y(:,1),y(:,2))
ylabel('i [A]')
xlabel('time [sec]')
grid
h2=figure;
plot(y(:,1),y(:,5))
ylabel('v [m/sec]')
xlabel('time [sec]')
grid
h2=figure;
plot(y(:,1),y(:,6))
ylabel('x [m]')
xlabel('time [sec]')
grid
h2=figure;
plot(y(:,1),y(:,4))
ylabel('P_m [W]')
xlabel('time [sec]')
grid
h2=figure;
plot(y(:,1),y(:,7))
ylabel('F_em [N]')
xlabel('time [sec]')
grid
h2=figure;
plot(y(:,1),y(:,8))
ylabel('F_S [N]')
xlabel('time [sec]')
grid
h2=figure;
plot(y(:,1),y(:,9))
ylabel('F_f [N]')
xlabel('time [sec]')
grid
h2=figure;
plot(y(:,1),y(:,10))
ylabel('F_D [N]')
```

```
xlabel('time [sec]')
grid
h2=figure;
plot(y(:,1),y(:,7),'-',y(:,1),y(:,8),'*',y(:,1),y(:,9),'+',y(:,1),y(:,10),'.')
ylabel('Forces(New)')
xlabel('time [sec]')
grid
```

# VITA

Oly Paz was born in Punto Fijo, Venezuela. She received her Bachelor of Science degree in Electrical Engineering in January 1990 from Zulia University, in Maracaibo, Venezuela. After graduation, she worked for almost two years at Microtel, S.A., in Venezuela, as an engineer, installing and programming Private Branch Exchange. Between 1991 and 1993, she worked in Jantesa, S.A., a consulting engineering company, as a project engineer for the Venezuelan oil industry. Then, she became to teach as an assistant professor in the departments of Electrical Engineering at Zulia University and at Rafael Urdaneta University, since 1994, in Maracaibo, Venezuela. She arrived in the United States on October 2001, to join first the English language and then the master degree. She is currently a candidate for the degree of Master of Science in Electrical Engineering at Louisiana State University, which will be conferred in December 2004.